SAE 9254
AL FG Quenched and Tempered Steel
Iteration #44

Fatigue Behavior, Monotonic Properties
and
Microstructural Data

Prepared by:

D. McClaflin
and
A. Fatemi

Department of Mechanical, Industrial and
Manufacturing Engineering
The University of Toledo
Toledo, Ohio 43606

Prepared for:
The AISI Bar Steel Applications Group

September 2001

American Iron and Steel Institute
2000 Town Center, Suite 320
Southfield, Michigan 48075
tel: 248-945-4777
fax: 248-352-1740
www.autosteel.org

UNIT CONVERSION TABLE

Measure	SI Unit	US Unit	from SI to US	from US to SI
Length	mm	in	1 mm = 0.03973 in	1 in = 25.4 mm
Area	mm^2	in^2	1 mm^2 = 0.00155 in^2	1 in^2 = 645.16 mm^2
Load	kN	kip	1 kN = 0.2248 kip	1 kip = 4.448 kN
Torque	Nm	lb in	1 Nm = 8.8507 lb in	1 lb in = 0.1130 Nm
Stress	MPa	ksi	1 MPa = 0.14503 ksi	1ksi = 6.895 MPa

In SI Unit:

1 kN = 10^3 N 1 Pa = 1 N/m^2 1 MPa = 10^6 Pa = 1 N/mm^2 1GPa = 10^9 Pa

In US Unit:

1klb = 10^3 lb 1 psi = 1 lb/in^2 1 ksi = 10^3 psi

NOMENCLATURE

A	cross-sectional area
b, c	axial fatigue strength exponent, fatigue ductility exponent
n, n'	monotonic, cyclic strain hardening exponent
b_0, c_0	shear fatigue strength exponent, fatigue ductility exponent
n_0, n_0'	monotonic, cyclic shear strain hardening exponent
E	modulus of elasticity
G	modulus of rigidity or shear modulus
$G_{midlife}$	modulus of rigidity or shear modulus at midlife
HB, HRC	Brinell, Rockwell C-scale
K, K'	monotonic, cyclic strength coefficient
K_0, K_0'	monotonic, cyclic shear strength coefficient
$N_{50\%}$	number of cycles to midlife
$2N_f$	reversals to failure
$r_{midsection}$	radius to midsection
$r_{surface}$	outer radius
T_f	torque at fracture
T_u	ultimate torque
$\Delta\gamma$	total shear strain range
γ_e, γ_p, γ	elastic, plastic, total shear strain
$\Delta\gamma_p/2$, $\Delta\gamma_p$	plastic shear strain amplitude, range
$\Delta\gamma_e/2$, $\Delta\gamma_e$	elastic shear strain amplitude, range
γ_f, γ_f'	shear fracture strain, shear fracture ductility coefficient
$\gamma_{midsection}$, $\gamma_{surface}$	shear strain at midsection, surface of tube
τ	shear stress
τ_y	shear yeild strength
τ_u	shear ultimate strength
$\Delta\tau/2$, $\Delta\tau$	shear stress amplitude, range
τ_a, τ_m	alternating, mean shear stress
τ_f, τ_f'	shear fracture stress, shear fatigue strength coefficient
$\tau_{midsection}$, $\tau_{surface}$	shear stress at midsection, surface of tube
θ_a	alternating rotational displacement
ε_f'	axial fatigue ductility coefficient
σ_f'	axial fatigue strength coefficient

TABLE OF CONTENTS

I. EXPERIMENTAL PROGRAM

1.1 Material

The SAE 9254 AL FG, quenched and tempered steel was manufactured by Stelco. This material was delivered to the University of Toledo in round bar form. The bars were approximately 1.875 inch in diameter prior to machining. In Table 1, the chemical composition obtained by Stelco and reported by the University of Waterloo [1] can be seen. Table 2 lists the axial monotonic and cyclic properties obtained and reported by the University of Waterloo [1].

1.2 Specimen

In this study, identical round thin-walled tube specimens were used for the monotonic and fatigue tests. The specimen configuration and dimensions are shown in Figure 1. The specimens were machined from barstock in a CNC machine to the proper dimensions and tolerances. Without ungripping the specimen, the hole was rough drilled and then bored. They were then honed in a honing machine. After this, the specimens were ground and then sent for heat treatment. Finally, they were honed again.

The specimens were put in a lathe and rotated while three different grits of aluminum oxide lapping film were used for polishing. The grits used were 30μ, 15μ, and 3μ. The polishing was then finished using a rotating polishing wheel with a polishing compound resulting in a mirror finish. The rotation of the polishing wheel coincided with the specimen's longitudinal axis. The polished surfaces were carefully examined under

magnification to ensure complete removal of machine marks within the test section. The internal and external diameters were measured to the nearest 0.0001 inch. The external diameter was measured using a comparator fitted with a dial indicator, and the internal diameter was measured using a micrometer and a bore gage.

1.3 Apparatus

An Instron closed-loop servo-controlled hydraulic axial-torsion load frame and digital servo-controller were used to conduct the tests. The calibration of this system was verified prior to beginning the test program. The load cell used had a capacity of 8850 lb.in. in torsion and 22,480 lb axially. Hydraulically operated grips using universal tapered collets were employed to secure the specimens' ends in series with the load cell. Total shear strain was controlled for most tests using an Epsilon axial-torsion extensometer. The calibration of the extensometer was verified using a specimen fitted with strain gages and the calibration apparatus provided by the manufacturer. The extensometer had a gage length of 1 inch and had a shear strain angle range of ±2.5° (±5° angle of twist on 1.0 in. diameter Specimen). In order to protect the specimens' surface from the contact points of the extensometer, ASTM Standard E606 [2] recommends the use of transparent tape or epoxy to 'cushion' the attachment. For this study, it was found that application of three layers of transparent tape effectively cushioned the extensometer when the extensometer springs had been adjusted properly.

The load train (load cell, grips, specimen, and actuator) was checked for proper alignment. Misalignment can result from both tilt and offset between the central lines of the load train components. According to ASTM Standard E606 [2] , the maximum

bending strains should not exceed 5 % of the minimum axial strain range imposed during any test program. To test this, two arrays of four strain gages per array were arranged at the upper and lower ends of the uniform gage section. For each array, gages were equally spaced around the circumference of a 0.61-in. diameter specimen with uniform gage section. The maximum bending strain determined from the specimen fitted with strain gages was less than 20 microstrain. This value was well within the allowable ASTM limit.

1.4 Test Methods and Procedures

1.4.1 Monotonic torsion tests

Two specimens were used to obtain the monotonic properties. Due to the limitations of the extensometer, strain control was used only up to a shear strain of 0.04. After this point, the extensometer was removed and rotational displacement control was used until fracture. For the entire strain-controlled portion (0 to 0.04 shear strain), a strain rate of 0.0002 shear strain/min was chosen. After this a rotation rate of 0.07 degrees/sec. was chosen to give a similar strain rate. For these tests the axial channel was run in load control allowing the specimen to change in length and avoiding axial stress.

1.4.2 Constant amplitude torsion fatigue tests

There are no ASTM standards for torsion fatigue testing. ASTM Standard E606 [2] for axial strain-controlled fatigue testing recommends at least 10 specimens be used to generate the axial fatigue properties of a material. For this torsion study, 14 specimens at 7 different shear strain amplitudes ranging from 0.0065 to 0.023 were utilized resulting in

lives between one hundred and one million cycles. The Instron software Max was used to record the hysteresis loops at intervals of 2^n.

There were three control modes used for these tests. Strain control was used for most tests, with the exception of the totally elastic tests. Most of the strain-controlled tests were run in strain control until the estimated midlife and then changed over to torque or rotation control. The reason for the change in control mode was for the protection of the extensometer. Since the material used was very brittle, fracture occurred suddenly and induced a shock to the extensometer. For the strain-controlled tests, the applied frequencies ranged from 0.10 Hz to 0.50 Hz. For the torque and rotation controlled tests, the frequencies ranged from 0.1 to 3 Hz. For some tests, after switching to torque or rotation control the frequency was increased in order to shorten the overall test duration. All tests were conducted at room temperature and using a sinusoidal waveform.

II. EXPERIMENTAL RESULTS AND ANALYSIS

2.1 Monotonic Deformation Behavior

The properties determined from monotonic tests were the following: modulus of rigidity or shear modulus (G), shear yield strength (τ_y), ultimate shear strength (τ_u), shear fracture strength (τ_f), shear strength coefficient (K_0), and shear strain hardening exponent (n_0).

Shear stress (τ), strain (γ), and plastic strain (γ_p) for the specimen midsection were calculated from the measured torque and the specimen dimensions:

$$\tau_{\text{midsection}} = \frac{T}{A\, r_{\text{midsection}}} \tag{1a}$$

$$\gamma_{\text{midsection}} = \gamma_{\text{surface}} \left(\frac{r_{\text{midsection}}}{r_{\text{surface}}} \right) \tag{1b}$$

$$\gamma_{\text{p\_midsection}} = \gamma_{\text{midsection}} - \frac{\tau_{\text{midsection}}}{G} \tag{1c}$$

Note that the difference between $\tau_{\text{midsection}}$ calculated from Equation (1a) and from $\tau = Tr/J$ for a thin-walled tube with outside and inside diameters of 0.6 and 0.5, respectively, is less than 1%. Either equation can be used for elastic as well as inelastic behavior. Equation (1b) is used to extrapolate the surface shear strain controlled in the test to the midsection shear strain. This linear extrapolation applies to both elastic as well as inelastic deformations.

The modulus of rigidity or shear modulus (G) was determined by calculating the slope of the elastic region of the monotonic curves. Therefore,

$$G = \frac{\Delta\tau_{\text{surface}}}{\Delta\gamma_{\text{surface}}} \tag{2}$$

The shear yield strength (τ_y) was determined by using the 0.2% offset method on the monotonic shear stress-strain curve. The ultimate shear strength (τ_u) and shear fracture strength were calculated using:

$$\tau_u = \frac{T_u}{A\, r_{\text{midsection}}} \tag{3}$$

and

$$\tau_f = \frac{T_f}{A\, r_{\text{midsection}}} \tag{4}$$

respectively, where T_u is the ultimate or maximum torque and T_f is the torque at fracture. Shear fracture strain (γ_f) was not attained because the extensometer was removed before fracture.

Analogous to axial stress-strain representation, the shear stress (τ) - shear strain (γ) relation is also often represented by the Ramberg-Osgood equation:

$$\gamma = \gamma_e + \gamma_p = \frac{\tau}{G} + \left(\frac{\tau}{K_0}\right)^{\frac{1}{n_0}} \tag{5}$$

The shear strength coefficient, K_0, and strain hardening exponent, n_0, are the intercept and slope of the best line fit to shear stress (τ) versus plastic shear strain (γ_p) data in log-log scale:

$$\tau = K_0 (\gamma_p)^{n_0} \tag{6}$$

The shear stress and plastic shear strain used were for the specimen midsection. When performing the least squares fit, the plastic shear strain (γ_p) was the independent variable

and the stress (τ) was the dependent variable in accordance with ASTM Standard E739 [3]. Figure 2 shows the torque versus rotation curves from monotonic tests. The monotonic shear stress-strain curves are shown in Figure 3. As can be seen from this figure, the two curves are close to each other. The plot used to determine K_0 and n_0 can be seen in Figure 4. The valid data range used was between the end of the yield point strain and the shear strain at which the extensometer was removed. A summary of the results from each monotonic torsion test is shown in Table A.1 and the average values are also listed in Table 5.

2.2 Cyclic Deformation Behavior

2.2.1 Transient cyclic response

Transient cyclic response describes the process of cyclic-induced change in deformation resistance of a material. Data obtained from constant amplitude fatigue tests were used to determine this response. Plots of stress amplitude variation versus applied number of cycles in strain-controlled tests can indicate the degree of transient cyclic softening/hardening. Also, these plots show when cyclic stabilization occurs. A composite plot of the transient normalized cyclic response for SAE 9254 AL FG quenched and tempered steel is shown in the rectangular plot in Figure A1, while a semi-log plot is shown in Figure A2. These figures indicate cyclic stability is achieved early during the cyclic deformation process. Even though multiple tests were conducted at each strain amplitude level, results from one test at each level are shown in these figures.

2.2.2 Steady-state cyclic deformation

Another cyclic behavior of interest was the steady state or stable response. Data obtained from constant amplitude fatigue tests were also used to determine this response. The properties determined from the steady-state hysteresis loops were the following: cyclic shear strength coefficient (K_0'), and cyclic shear strain hardening exponent (n_0'). Half-life (midlife) hysteresis loops and data were used to obtain the stable cyclic shear properties. Similar to monotonic behavior, the cyclic shear stress-strain behavior can be characterized by the Ramberg-Osgood type equation:

$$\gamma_a = \gamma_e + \gamma_p = \frac{\tau_a}{G} + \left(\frac{\tau_a}{K_0'}\right)^{\frac{1}{n_0'}} \tag{7}$$

It should be noted that in Equation (7) and the other equations that follow, G is the shear modulus that was measured from the monotonic tests. The cyclic shear strength coefficient, K_0', and cyclic shear strain hardening exponent, n_0', are the intercept and slope of the best line fit to shear stress amplitude ($\Delta\tau/2$) versus plastic shear strain amplitude ($\Delta\gamma_p/2$) data in log-log scale:

$$\frac{\Delta\tau}{2} = K_0'\left(\frac{\gamma_p}{2}\right)^{n_0'} \tag{8}$$

When performing the least squares fit, the plastic shear strain amplitude ($\Delta\gamma_p/2$) was the independent variable and the shear stress amplitude ($\Delta\tau/2$) was the dependent variable as is done for axial testing in accordance with ASTM Standard E739. Shear stress amplitudes were calculated from Equation (1a) for specimen midsection at or near

midlife. Plastic shear strain amplitudes for midsection were calculated by the following equation:

$$\left(\frac{\Delta\gamma_p}{2}\right)_{\text{midsection}} = (\gamma_a)_{\text{midsection}} - \frac{(\tau_a)_{\text{midsection}}}{G_{\text{midlife}}} \tag{9}$$

This plot is shown in Figure 5. To generate the K_0' and n_0' values, the range of data used in the figure was chosen for $[\Delta\gamma_p/2]_{\text{calculated}} \geq 0.00027$. The curve showing the Ramberg-Osgood equation and the data can be seen in Figure 6.

The cyclic stress-strain curve reflects the resistance of a material to cyclic deformation and can be vastly different from the monotonic stress - strain curve. In Figure 7, superimposed plots of monotonic and cyclic curves are shown. As can be seen in Figure 7, SAE 9254 AL FG quenched and tempered steel cyclically softens. Figure A3 shows a composite plot of the steady-state (midlife) hysteresis loops. Even though multiple tests were conducted at each level, the loop from only one test is shown from each shear strain level. Tables 3 and 4 provide the summary of the fatigue test results and fatigue test calculations, respectively.

2.3 Constant Amplitude Torsional Fatigue Behavior

Constant amplitude strain-controlled torsion fatigue tests were performed to determine the shear strain-life curve. Analogous to the Coffin-Manson equation for axial fatigue behavior, the following equation relates the shear strain amplitude to the fatigue life:

$$\frac{\Delta\gamma}{2} = \frac{\Delta\gamma_e}{2} + \frac{\Delta\gamma_p}{2} = \frac{\tau_f'}{G}(2N_f)^{b_0} + \gamma_f'(2N_f)^{c_0} \tag{10}$$

where τ_f' is the shear fatigue strength coefficient, b_0 is the shear fatigue strength exponent, γ_f' is the shear fatigue ductility coefficient, c_0 is the shear fatigue ductility exponent, G is the shear modulus, and $2N_f$ is the number of reversals to failure (which was defined as a 10% torsional load drop).

The shear fatigue strength coefficient, τ_f', and shear fatigue strength exponent, b_0, are the intercept and slope of the best line fit to shear stress amplitude ($\Delta\tau/2$) versus reversals to failure ($2N_f$) data in log-log scale:

$$\frac{\Delta\tau}{2} = \tau_f'(2N_f)^{b_0} \tag{11}$$

When performing the least squares fit, the shear stress amplitude ($\Delta\tau/2$) was the independent variable and the reversals to failure ($2N_f$) was the dependent variable as is done for axial testing in accordance with ASTM Standard E739 [3]. This plot is shown in Figure 8. To generate the τ_f' and b_0 values, the range of data used in this figure was chosen for $N_f \leq 10^6$ cycles. The shear fatigue ductility coefficient, γ_f', and shear fatigue ductility exponent, c_0, are the intercept and slope of the best line fit to calculated shear plastic strain amplitude ($\Delta\gamma_p/2$) versus reversals to failure ($2N_f$) data in log-log scale:

$$\left(\frac{\Delta\gamma_p}{2}\right)_{calculated} = \gamma_f'(2N_f)^{c_0} \tag{12}$$

when performing the least squares fit, the calculated shear plastic strain amplitude ($\Delta\gamma_p/2$) was the independent variable and the reversals to failure ($2N_f$) was the dependent variable as is done in axial testing in accordance with ASTM Standard E739 [2]. The calculated shear plastic strain amplitude was determined from Equation 12. This plot is shown in Figure 9. Figure 10 shows the same plot with measured plastic shear strain amplitude

values. As can be seen, similar results are obtained. To be consistent with the procedure used for axial strain-controlled fatigue property determinations by AISI, the plot with the calculated plastic shear strain amplitudes was used to obtain γ_f' and c_0. The data range used in these plots was for $\Delta\gamma_p/2 > 0.00067$.

The total shear strain amplitude versus reversals to failure plot is shown in Figure 11. This plot displays the shear strain-life curve (Eqn. 10), the elastic shear strain portion (Eqn. 11), the plastic shear strain portion (Eqn. 12), and superimposed torsion fatigue data. A summary of the cyclic properties for SAE 9254 AL FG quenched and tempered steel is provided in Table 5.

III. PREDICTIONS AND FAILURE MECHANISMS

3.1 Predictions from axial data

Common failure criteria were used to predict the torsional behavior of the material from axial data. Experimentally obtained monotonic and cyclic data for both axial and torsional tests of the material are summarized in Table 6. The torsional monotonic curve was compared to the von Mises and the Tresca predictions. This was done by using the Ramberg-Osgood equation:

$$\gamma = \gamma_e + \gamma_p = \frac{\tau}{G} + \left(\frac{\tau}{K_0}\right)^{\frac{1}{n_0}} \tag{13}$$

where K_0 and n_0 are computed using predictions based on von Mises criterion [3]:

$$K_0 = K(1/3)^{(n+1)/2} \quad \text{and} \quad n_0 = n \tag{14}$$

resulting in K_0=1645 and n_0=0.0418, and predictions based on Tresca criterion:

$$K_0 = \frac{K}{2}(2/3)^n \quad \text{and} \quad n_0 = n \tag{15}$$

resulting in K_0 = 1433 MPa and n_0 = 0.0418. Note that from the torsion test, K_0 = 1416 and n_0 = 0.0473. This comparison can be seen in Figure 12. It can be seen from this figure that the Tresca estimation fits the actual data better than the von Mises prediction.

The next prediction is for the cyclic deformation curve. This was done using the same equations as with the monotonic curves (Equations 14 and 15), except with n_0' and K_0' being calculated using n' and K' from the axial cyclic properties. The von Mises criterion results in K_0' = 1827 MPa, and n_0' = 0.088, while the Tresca criterion results in K_0' = 1603 MPa, and n_0' = 0.088. Note that from the torsion test data K_0' = 1277 MPa,

and $n_0' = 0.0783$. These constants were then used in the following equation to represent the shear stress-shear strain relationship:

$$\gamma_a = \gamma_e + \gamma_p = \frac{\tau_a}{G} + \left(\frac{\tau_a}{K_0'}\right)^{\frac{1}{n_0'}} \tag{16}$$

This comparison can be seen in Figure 13. This figure shows that both estimates are high compared to the test data, with Tresca criterion providing better estimations. It should be noted, however, that as mentioned earlier, both Tresca and von Mises criteria use axial properties to predict torsional behavior. For the material studies, due to small cyclic plastic deformations in axial tests and lack of sufficient data, reported values of K' and n' may not be accurate. Therefore, less accurate predictions for the cyclic curve, compared to the monotonic curve, may be due to insufficient data from the axial tests, rather than low predictive capability of the criterion.

The final predictions made were for the fatigue data. The torsional strain-life equation:

$$\frac{\Delta\gamma}{2} = \frac{\Delta\gamma_e}{2} + \frac{\Delta\gamma_p}{2} = \frac{\tau_f'}{G}(2N_f)^{b_0} + \gamma_f'(2N_f)^{c_0} \tag{17}$$

was used, where τ_f' and γ_f' were calculated for the von Mises criteria using:

$$\tau_f' = \sigma'_f / \sqrt{3}, \qquad \gamma_f' = \sqrt{3}\varepsilon_f', \quad b_0 = b, \text{ and } \quad c_0 = c \tag{18}$$

resulting in $\tau_f' = 2372$ MPa, $\gamma_f' = 1.96$, $b_0 = -0.109$, and $c_0 = -0.954$. For the Tresca criterion:

$$\tau_f' = \sigma'_f / 2, \qquad \gamma_f' = 1.5\varepsilon_f', \quad b_0 = b, \text{ and } \quad c_0 = c \tag{19}$$

were used resulting in $\tau_f' = 2054$ MPa, $\gamma_f' = 1.69$, $b_0 = -0.109$, and $c_0 = -0.954$. For the maximum principal strain criterion:

$$\tau_f' = \sigma'_f/(1+\nu), \qquad \gamma_f' = 2\varepsilon_f', \qquad b_0 = b, \text{ and } \qquad c_0 = c \tag{20}$$

resulting in $\tau_f' = 2739$ MPa, $\gamma_f' = 2.26$, $b_0 = -0.109$, and $c_0 = -0.954$. Note that from torsion tests $\tau_f' = 1255$ MPa, $\gamma_f' = 0.4001$, $b_0 = -0.0544$, and $c_0 = -0.6027$. This comparison can be seen in Figure 14. It can be seen that among the three criteria the von Mises criterion provides the best estimation.

3.2 Predictions from Hardness

A simple method for the estimation of axial fatigue properties from Brinell hardness and elastic modulus of steels has been proposed by Roessle and Fatemi [5]. This method is valid for hardness between 150 and 700HB and uses the following estimates:

$$\sigma_f' = 4.25(HB) + 225 \tag{21}$$

$$\varepsilon_f' = \frac{1}{E}\left[0.32(HB)^2 - 487(HB) + 191000\right] \tag{22}$$

$$b_0 = -0.09, \qquad \text{and} \qquad c_0 = -0.56 \tag{23}$$

A comparison of the predicted axial fatigue curve with the experimental axial curve is shown in Figure 15. Combining Equations (21) through (23) with Equations (17) through (20) gives three new estimations of torsional fatigue properties based on hardness. The substitution for von Mises criterion results in:

$$\frac{\Delta\gamma}{2} = \frac{[4.25(HB)+225]}{\sqrt{3}G}(2N_f)^{-0.09} + \frac{\sqrt{3}}{E}[0.32(HB)^2 - 487(HB) + 191000](2N_f)^{-0.56} \tag{24}$$

for Tresca criterion:

$$\frac{\Delta\gamma}{2}=\frac{[4.25(HB)+225]}{2G}(2N_f)^{-0.09}+\frac{1.5}{E}[0.32(HB)^2-487(HB)+191000](2N_f)^{-0.56} \tag{25}$$

and for maximum principal strain criterion:

$$\frac{\Delta\gamma}{2}=\frac{[4.25(HB)+225]}{G(1+\nu)}(2N_f)^{-0.09}+\frac{2}{E}[0.32(HB)^2-487(HB)+191000](2N_f)^{-0.56} \tag{26}$$

This comparison can be seen in Figure 16. Although it appears that the maximum principal strain criterion fits the data the best, it is invalid to conclude that it is the best prediction. Referring back to Figure 15, it can be seen that the predictions from hardness are low compared to the data. Therefore the closeness of the maximum principal strain prediction is merely a cancellation of two errors. One error is that of the low estimate from the hardness prediction method and the other being that of high estimate from the maximum principal strain criterion.

3.3 Failure Modes and Fracture Surfaces

Observed cracks on the specimens appeared to be in one of the maximum shear planes, either parallel to the axis of the specimen or circumferential in orientation. Due to the high hardness and brittleness of the material tested, it was difficult to stop the tests before fracture. Figure 17 shows a specimen for which it was possible to stop the experiment before fracture occurred. The long longitudinal crack can be seen here. In Figure 18, the specimen shown had a longitudinal fatigue crack until brittle fracture occurred. The specimen in Figure 19 shows cracking on both longitudinal and transverse planes, with final fracture occurring in a spiral shape on a 45° plane (maximum principal stress plane). Figure 20 shows a fractured specimen with a circumferential crack. One

conclusion that can be drawn from these observations is that the orientation of fatigue cracks under purely torsional loading was on the maximum shear planes. It should also be noted that when this material fractures, although the failure crack may appear to be on the maximum principal stress plane at 45°, the fatigue damage mechanism in fact is shear. This agrees with the fact that, contrary to common belief, stress or strain criteria may not be appropriate for brittle/high strength steels and can result in conservative fatigue life predictions.

REFERENCES

[1] Khalil, M., Topper, T. H., "Fatigue Behavior, Monotonic Properties and Microstructure Data for SAE 9254 AL FG, Quenched and Tempered." Department of Civil Engineering, University of Waterloo, July 1999.

[2] ASTM Standard E739-91, "Standard Practice for Statistical Analysis of Linear or Linearized Stress-Life (S-N) and Strain-Life (ε-N) Fatigue Data," Annual Book of ASTM Standards, Vol. 03.01, 1995, pp. 615-621.

[3] ASTM Standard E606-92, "Standard Practice for Strain-Controlled Fatigue Testing," Annual Book of ASTM Standards, Vol. 03.01, 1997, pp. 198-206.

[4] Dowling, N. E., "Mechanical Behavior of Materials: Engineering Methods for Deformation, Fracture, and Fatigue," 2nd Edition, Prentice-Hall, Inc., 1999.

[5] Roessle ML, Fatemi, A., "Strain-controlled fatigue properties of steels and some simple approximations," International Journal of Fatigue, Vol. 22, 2000, pp. 495-511.

Table 1: Chemical composition of SAE 9254 AL FG Quenched and Tempered steel [1]

Carbon, C	0.57%
Manganese, Mn	0.71%
Phosphorous, P	0.011%
Sulfur, S	0.009%
Silicon, Si	1.57%
Copper, Cu	0.011%
Nickel, Ni	0.01%
Chromium, Cr	0.72%
Molybdenum, Mo	0.005%
Vanadium, Va	0.007%
ASA	0.028%
N	0.007%
Columbium, Cb	0.002%

Table 2: Axial Material Properties [1]

Monotonic Properties for SAE 9254 AL FG, Quenched and Tempered steel.

Average Elastic Modulus, E	=	205.4	GPa
Yield Strength	=	2270	MPa
Ultimate tensile Strength	=	2950	MPa
% Elongation	=	3.92	%
% Reduction of Area	=	3.99	%
True fracture strain, $Ln\ (A_i / A_f)$	=	4.08	%
True fracture stress, $\sigma_f = \frac{P_f}{A_f}$	=	2483	MPa
Bridgman correction, $\sigma_f = \frac{P_f}{A_f} \Big/ \left(1+\frac{4R}{D_f}\right) Ln\left(1+\frac{D_f}{4R}\right)$	=	2047	MPa
Monotonic strength coefficient, K	=	2916	MPa
Monotonic strain hardening exponent, n	=	0.0418	
Hardness, Rockwell C (HRC)	=	58	
Hardness, Brinell	=	584	

Cyclic Properties for SAE 9254 AL FG, Quenched and Tempered steel.

Cyclic Yield Strength, (0.2% offset)= $K'(0.002)^{n'}$	=	1922	MPa
Cyclic strength coefficient, K'	=	3322	MPa
Cyclic strain hardening exponent, n'	=	0.088	
Fatigue Strength Coefficient, σ'_f	=	4108	MPa
Fatigue Strength Exponent, b	=	-0.109	
Fatigue Ductility Coefficient, ε'_f	=	1.13	
Fatigue Ductility Exponent, c	=	-0.954	

P_f:	Load at fracture.
A_i and A_f:	Specimen cross-section area before and after fracture.
R:	Specimen neck radius.
D_f	Specimen diameter at fracture.

Table 3: Torsion fatigue test results

Specimen									Mid-Life measurements						
Type	Number	OD, mm (in.)	ID, mm (in.)	Test Date	$G_{initial}$, MPa (ksi)	Control Mode	Frequency, Hz	$N_{50\%}$ cycles	$\gamma_{a\ surface}$	$_{m\ surface}$	T_a, Nm (in. Lb.)	T_m, Nm (in. Lb.)	θ_a, degrees	N_f, cycles	Notes
Tube	T 16	15.43 (0.6076)	12.67 (0.4989)	5/30/01	80,869 (11,729)	Strain/Rotation	0.1	70	0.02342	0.00053	394 (3,487)	2 (22)	8.10	127	
Tube	T 10	15.45 (0.6081)	12.67 (0.4990)	6/1/01	79,848 (11,581)	Rotation	0.1	64	0.02321	0.00020	395 (3,493)	0 (2)	7.72	195	
Tube	T 5	15.34 (0.6038)	12.59 (0.4958)	4/7/01	n/a	Strain	0.1	128	0.02309	0.00000	349 (3,089)	1 (11)	7.61	289	
Tube	T 7	15.44 (0.6078)	12.79 (0.5035)	4/6/01	n/a	Strain	0.3	512	0.01501	-0.00003	330 (2,924)	0 (2)	5.67	1,051	
Tube	T 19	15.43 (0.6075)	12.73 (0.5012)	5/23/01	87,494 (12,690)	Strain/Torque	0.3	512	0.01500	0.00000	348 (3,083)	0 (2)	5.79	804	
Tube	T 14	15.45 (0.6081)	12.75 (0.5020)	5/24/01	81,434 (11,811)	Strain	0.4	2,048	0.01154	0.00003	314 (2,783)	2 (18)	4.66	3,418	
Tube	T 3	15.39 (0.6059)	12.67 (0.4988)	4/9/01	n/a	Strain	0.4	4,096	0.01149	-0.00057	304 (2,695)	0 (3)	4.44	7,088	
Tube	T 22	15.49 (0.6099)	12.65 (0.4979)	5/31/01	78,111 (11,329)	Strain/Rotation	0.5	4,324	0.01004	0.00003	298 (2,640)	7 (61)	4.16	12,669	
Tube	T 1	15.43 (0.6074)	12.70 (0.5002)	4/4/01	n/a	Strain	0.5	10,169	0.01003	0.00000	295 (2,609)	-3 (27)	4.08	20,286	
Tube	T 8	15.47 (0.6093)	12.64 (0.4978)	5/8/01	n/a	Strain	0.5	8,192	0.00899	-0.00001	286 (2,533)	73 (644)	3.89	17,757	not used
Tube	T 20	15.43 (0.6075)	12.75 (0.5019)	5/25/01	82,110 (11,909)	Strain/Torque	0.5	2,048	0.00884	0.00005	278 (2,464)	-4 (37)	3.78	6,826	not used
Tube	T 18	15.47 (0.6090)	12.75 (0.5020)	5/25/01	n/a	Torque	2	32,768	0.00800	0.00000	250 (2,214)	0 (1)	3.39	58,859	
Tube	T 11	15.45 (0.6081)	12.67 (0.4989)	6/1/01	n/a	Torque	3	16,384	0.00800	0.00000	253 (2,239)	0 (0)	3.40	38,503	
Tube	T 17	15.47 (0.6091)	12.67 (0.4990)	6/10/01	n/a	Torque	2	32,768	0.00700	0.00000	224 (1,979)	0 (0)	2.98	79,522	
Tube	T 9	15.46 (0.6086)	12.67 (0.4990)	6/14/01	n/a	Torque	2	32,768	0.00700	0.00000	222 (1,969)	0 (0)	3.00	60,663	
Tube	T 13	15.48 (0.6095)	12.66 (0.4986)	6/10/01	n/a	Torque	2	524,288	0.00650	0.00000	209 (1,850)	0 (1)	2.80	>1,007,232	runout test

Table 4: Torsion fatigue test calculation results

Specimen					Midlife Values											
					Surface						Midsection					
Type	Number	$G_{first\ cycle}$, Mpa (ksi)	$2N_{50\%}$	$G_{midlife}$, Mpa (ksi)	γ_a	γ_m	$(\Delta\gamma_p/2)_{meas}$	$(\Delta\gamma_p/2)_{calc}$	τ_a, Mpa (ksi)	τ_m, MPa (ksi)	γ_a	γ_m	$(\Delta\gamma_p/2)_{calc}$	τ_a, MPa (ksi)	τ_m, MPa (ksi)	$2N_f$
Tube	T 16	81,861 (11,873)	140	74,877 (10,860)	0.02342	0.00053	0.00989	0.01096	933 (135)	6 (1)	0.02132	0.00048	0.00904	920 (133)	6 (1)	254
Tube	T 10	77,718 (11,272)	128	73,291 (10,630)	0.02321	0.00020	0.00939	0.01052	930 (135)	1 (0)	0.02113	0.00018	0.00861	917 (133)	0 (0)	390
Tube	T 5	78,049 (11,320)	256	73,981 (10,730)	0.02309	0.00000	0.01069	0.01170	842 (122)	-3 (0)	0.02102	0.00000	0.00979	831 (120)	3 (0)	578
Tube	T 7	81,365 (11,801)	1024	77,370 (11,222)	0.01501	-0.00003	0.00387	0.00449	814 (118)	1 (0)	0.01372	-0.00003	0.00342	797 (116)	1 (0)	2,102
Tube	T 19	85,557 (12,409)	1024	77,132 (11,187)	0.01500	0.00000	0.00351	0.00403	846 (123)	0 (0)	0.01369	0.00000	0.00295	828 (120)	0 (0)	1,608
Tube	T 14	82,282 (11,934)	4096	78,321 (11,360)	0.01154	0.00003	0.00132	0.00165	775 (112)	5 (1)	0.01053	0.00003	0.00099	747 (108)	5 (1)	6,836
Tube	T 3	76,394 (11,080)	8192	75,642 (10,971)	0.01149	-0.00057	0.00118	0.00156	751 (109)	1 (0)	0.01048	-0.00052	0.00091	724 (105)	1 (0)	14,176
Tube	T 22	78,910 (11,445)	8648	77,463 (11,235)	0.01004	0.00003	0.00057	0.00087	711 (103)	17 (2)	0.00912	0.00002	0.00044	672 (98)	15 (2)	25,338
Tube	T 1	77,504 (11,241)	20338	78,483 (11,383)	0.01003	0.00000	0.00041	0.00067	734 (106)	8 (1)	0.00914	0.00000	0.00027	696 (101)	-7 (1)	40,572
Tube	T 18	n/a	65536	n/a	0.00800	0.00000	0.00000	0 (0)	639 (93)	0 (0)	0.00730	0.00000	0 (0)	589 (85)	0 (0)	117,718
Tube	T 11	n/a	32768	n/a	0.00800	0.00000	0.00000	0 (0)	640 (93)	0 (0)	0.00728	0.00000	0 (0)	588 (85)	0 (0)	77,006
Tube	T 17	n/a	65536	n/a	0.00700	0.00000	0.00000	0 (0)	564 (82)	0 (0)	0.00637	0.00000	0 (0)	514 (75)	0 (0)	159,044
Tube	T 9	n/a	65536	n/a	0.00700	0.00000	0.00000	0 (0)	564 (82)	0 (0)	0.00637	0.00000	0 (0)	514 (75)	0 (0)	121,326
Tube	T 13	n/a	1048576	n/a	0.00650	0.00000	0.00000	0 (0)	524 (76)	0 (0)	0.00591	0.00000	0 (0)	477 (69)	0 (0)	>2,014,464

Table 5: Summary of torsion properties

Monotonic Properties	Average	
Modulus of Rigidity, G, GPa (ksi):	80.3	(11642.7)
Shear Yield Strength, τ_y, MPa (ksi):	1053.7	(152.8)
Shear ultimate strength, τ_u, MPa (ksi):	1224.8	(177.6)
Shear fracture strain, γ_f:	N/A	-
Shear fracture stress, τ_f, Mpa (ksi):	1010.6	(146.6)
Shear strength coefficient, K_0, MPa (ksi):	1437.5	(208.5)
Shear strain hardening exponent, n_0:	0.0507	-
Cyclic Properties		
Cyclic shear yield strength, τ_y' (0.2% offset) = $K_0'(0.002)^{n0'}$, MPa (ksi)	784.9	(113.8)
Cyclic shear strength coefficient, K_0', MPa (ksi):	1276.9	(185.2)
Cyclic shear strain hardening exponent, n_0':	0.0783	-
Fatigue shear strength coefficient, τ_f', MPa (ksi):	1254.9	(182.0)
Fatigue shear strength exponent, b_0:	-0.0544	-
Fatigue shear ductility coefficient, γ_f':	0.4001	-
Fatigue shear ductility exponent, c_0:	-0.6027	-

Table 6: Comparison of axial and torsional properties

Monotonic Properties	Axial			Torsional		
Modulus, GPa (ksi)	$E =$	205.4	(29789.2)	$G =$	80.3	(11642.7)
Yield Strength, MPa (ksi):	$\sigma_y =$	2270	(329.2)	$\tau_y =$	1053.7	(152.8)
Ultimate strength, MPa (ksi):	$\sigma_u =$	2950	(427.8)	$\tau_u =$	1224.8	(177.6)
Fracture strain:	$\varepsilon_f =$	4.08%	-	$\gamma_f =$	N/A	-
Fracture stress, Mpa (ksi):	$\sigma_f =$	2483	(360.1)	$\tau_f =$	1010.6	(146.6)
Strength coefficient, MPa (ksi):	$K =$	2916	(422.9)	$K_o =$	1437.5	(208.5)
Strain hardening exponent:	$n =$	0.0418	-	$n_o =$	0.0507	-
Cyclic Properties						
Cyclic yield strength, MPa (ksi)	$\sigma_y' =$	1922	(278.7)	$\tau_y' =$	784.9	(113.8)
Cyclic strength coefficient, MPa (ksi):	$K' =$	3322	(481.8)	$K_o' =$	1276.9	(185.2)
Cyclic strain hardening exponent:	$n' =$	0.088	-	$n_o' =$	0.0783	-
Fatigue strength coefficient, MPa (ksi):	$\sigma_f' =$	4108	(595.8)	$\tau_f' =$	1254.9	(182.0)
Fatigue strength exponent:	$b =$	-0.109	-	$b_o =$	-0.0544	-
Fatigue ductility coefficient:	$\varepsilon_f' =$	1.13	-	$\gamma_f' =$	0.4001	-
Fatigue ductility exponent:	$c =$	-0.954	-	$c_o =$	-0.6027	-

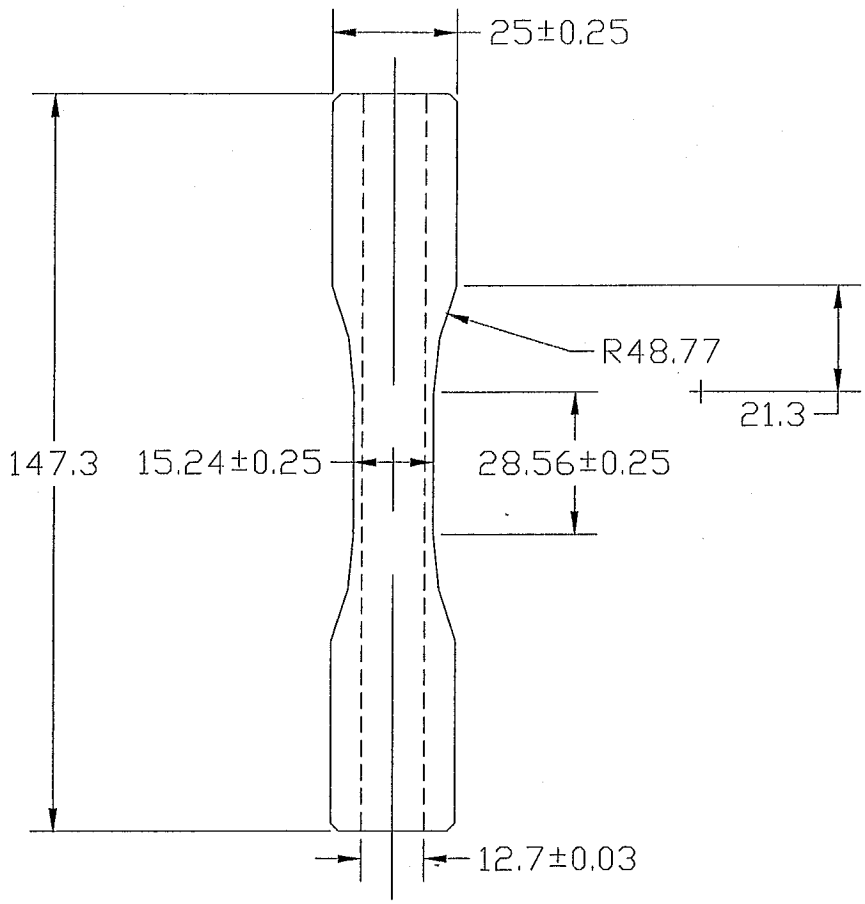

Figure 1: Specimen configuration and dimensions (all dimensions in milimeters)

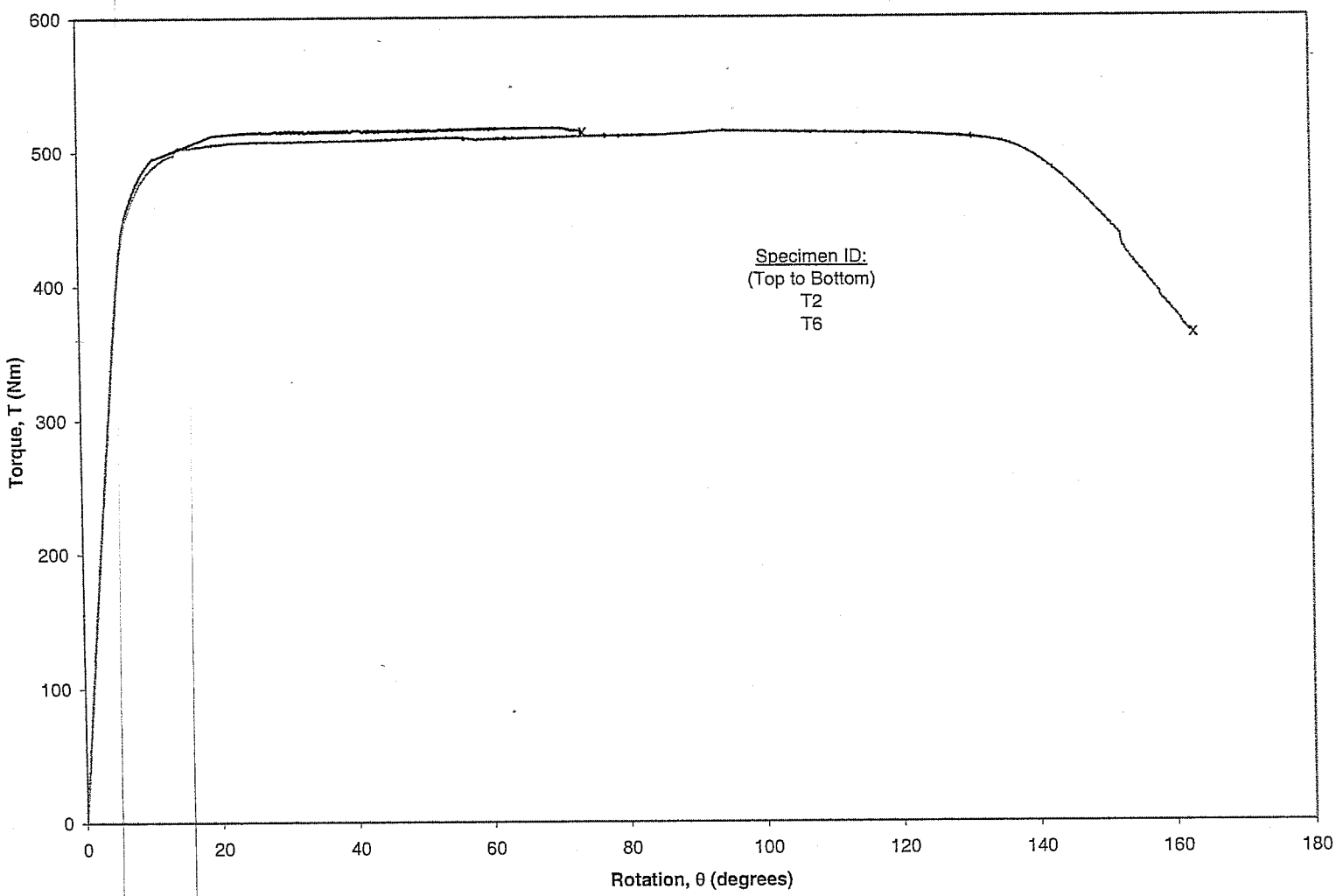

Figure 2: Monotonic torque versus rotation curves

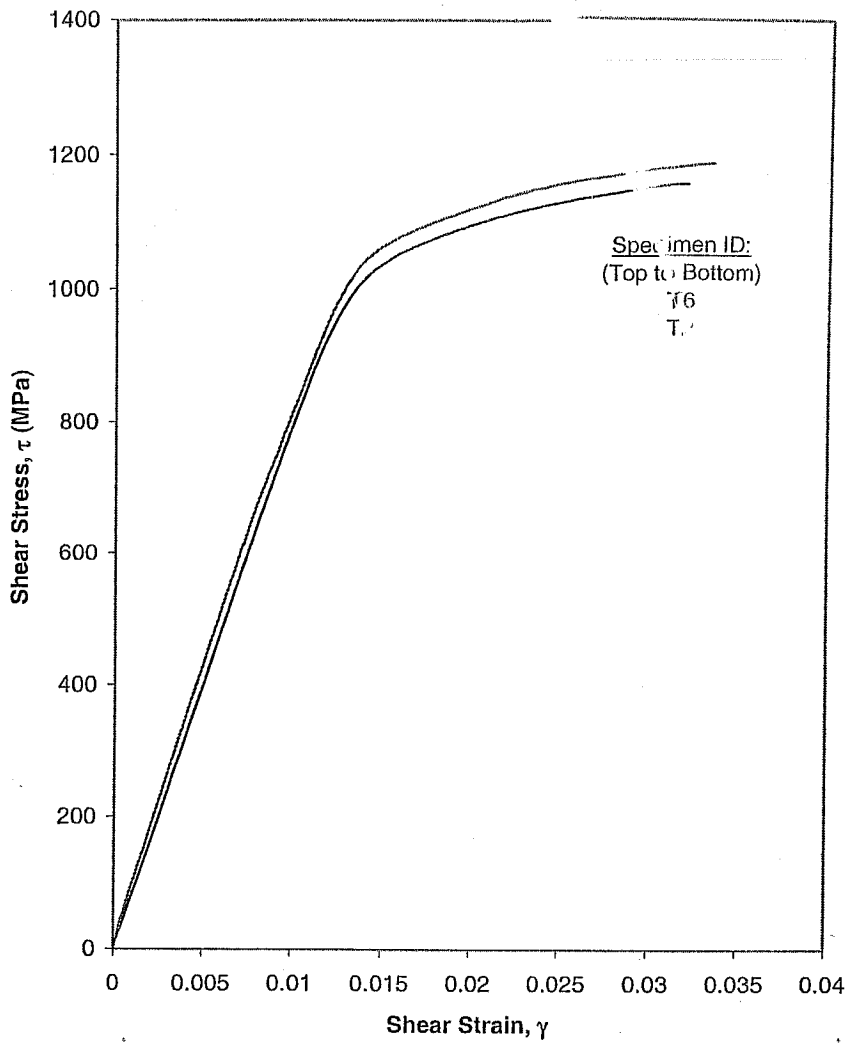

Figure 3: Monotonic shear stress-strain curves

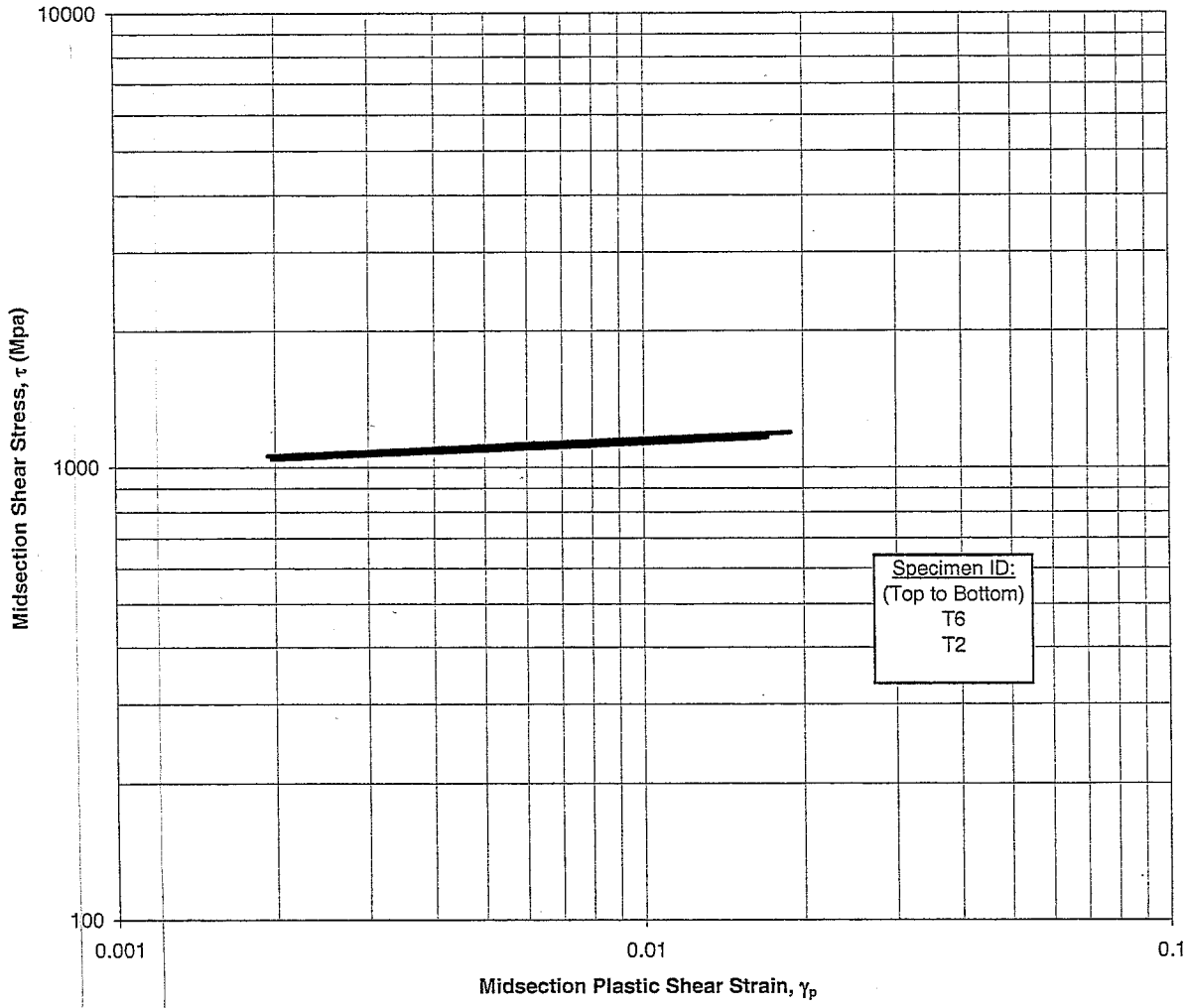

T6

$\tau = 1459.3\gamma_p^{0.0517}$

$K_0 = 1459.3$

$n_0 = 0.0517$

$R^2 = 0.9966$

T2

$\tau = 1415.7\gamma_p^{0.0496}$

$K_0 = 1415.7$

$n_0 = 0.0496$

$R^2 = 0.9974$

Figure 4: Shear stress versus plastic shear strain

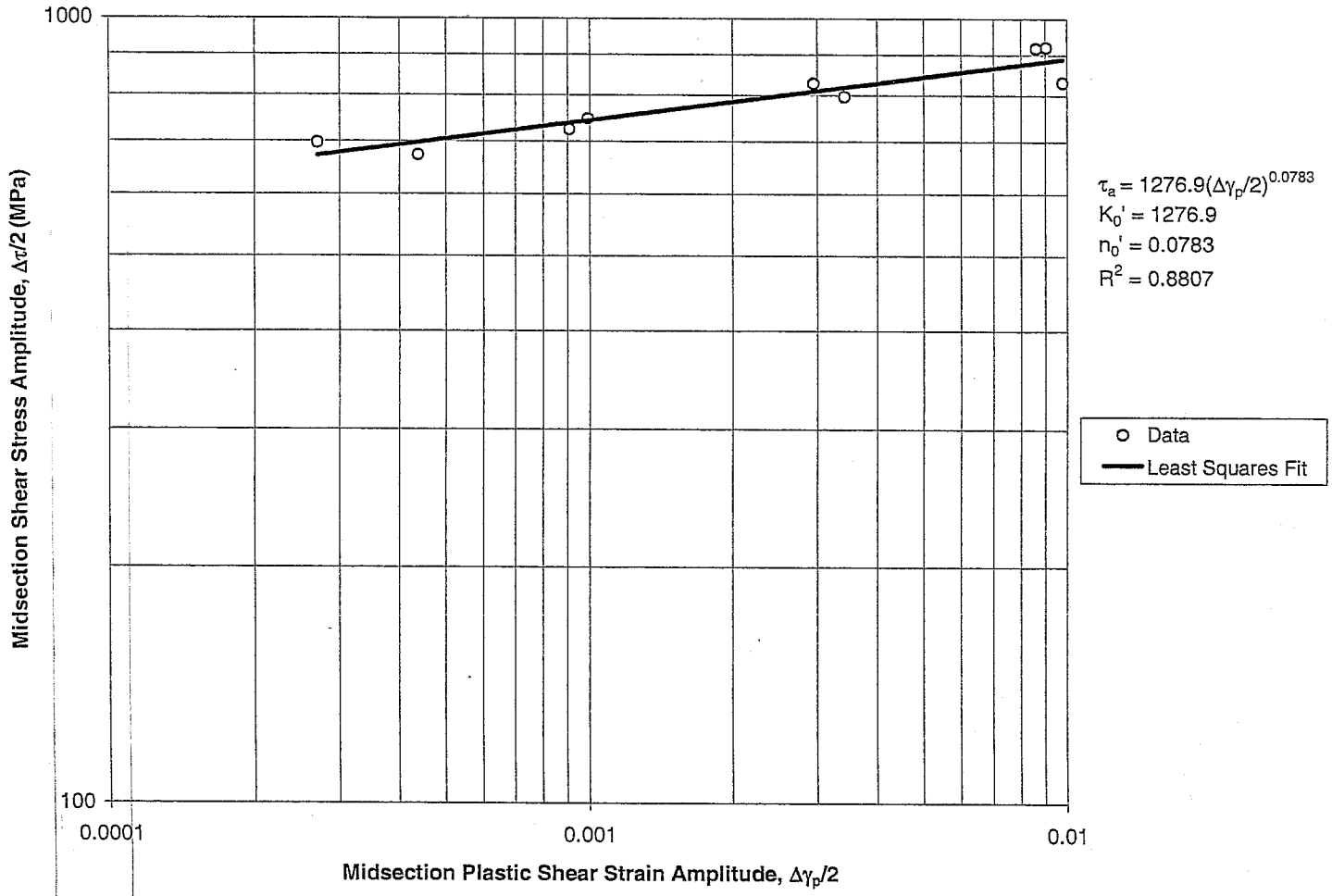

Figure 5: Shear stress amplitude versus plastic shear strain amplitude

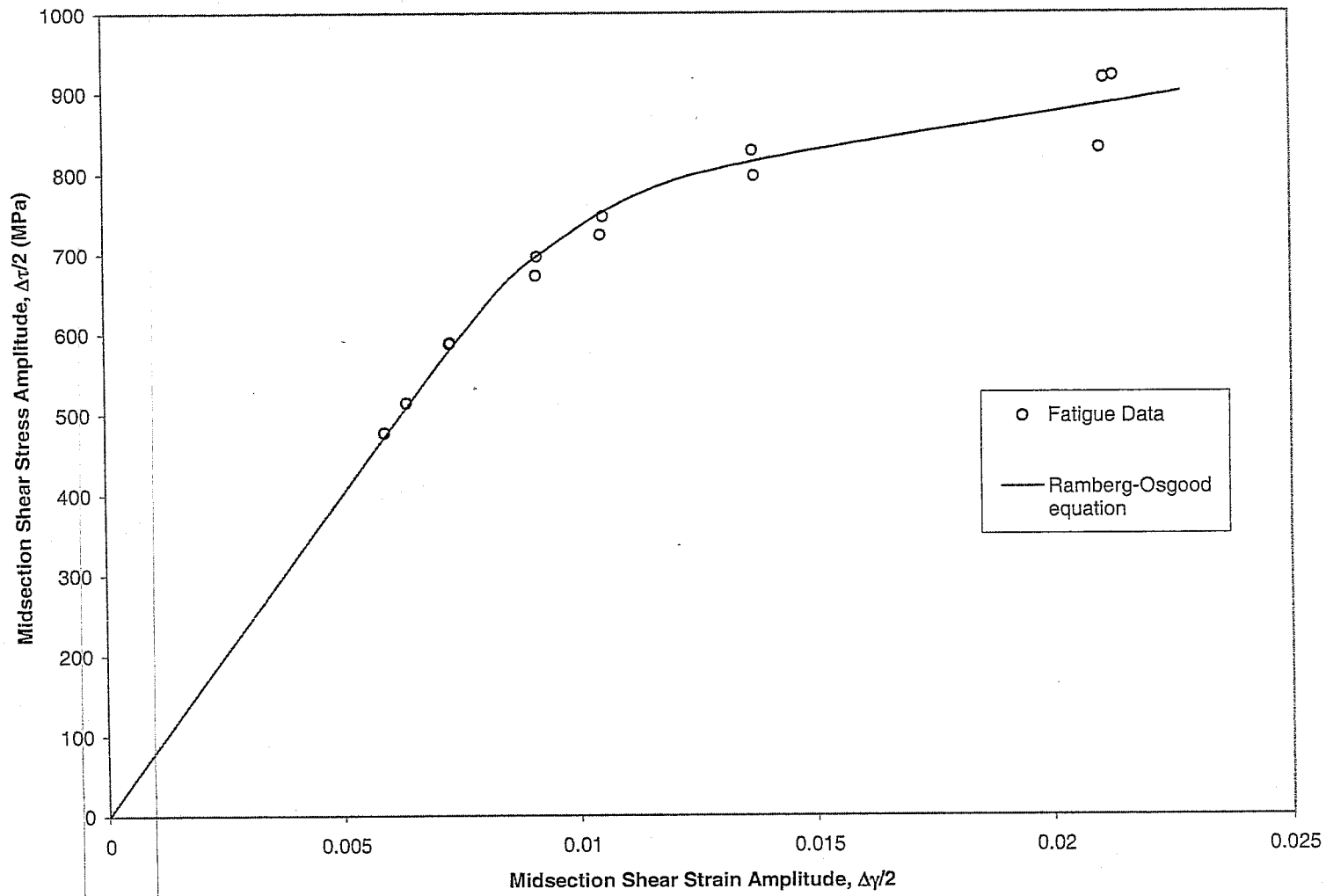

Figure 6: Shear stress amplitude versus shear strain amplitude

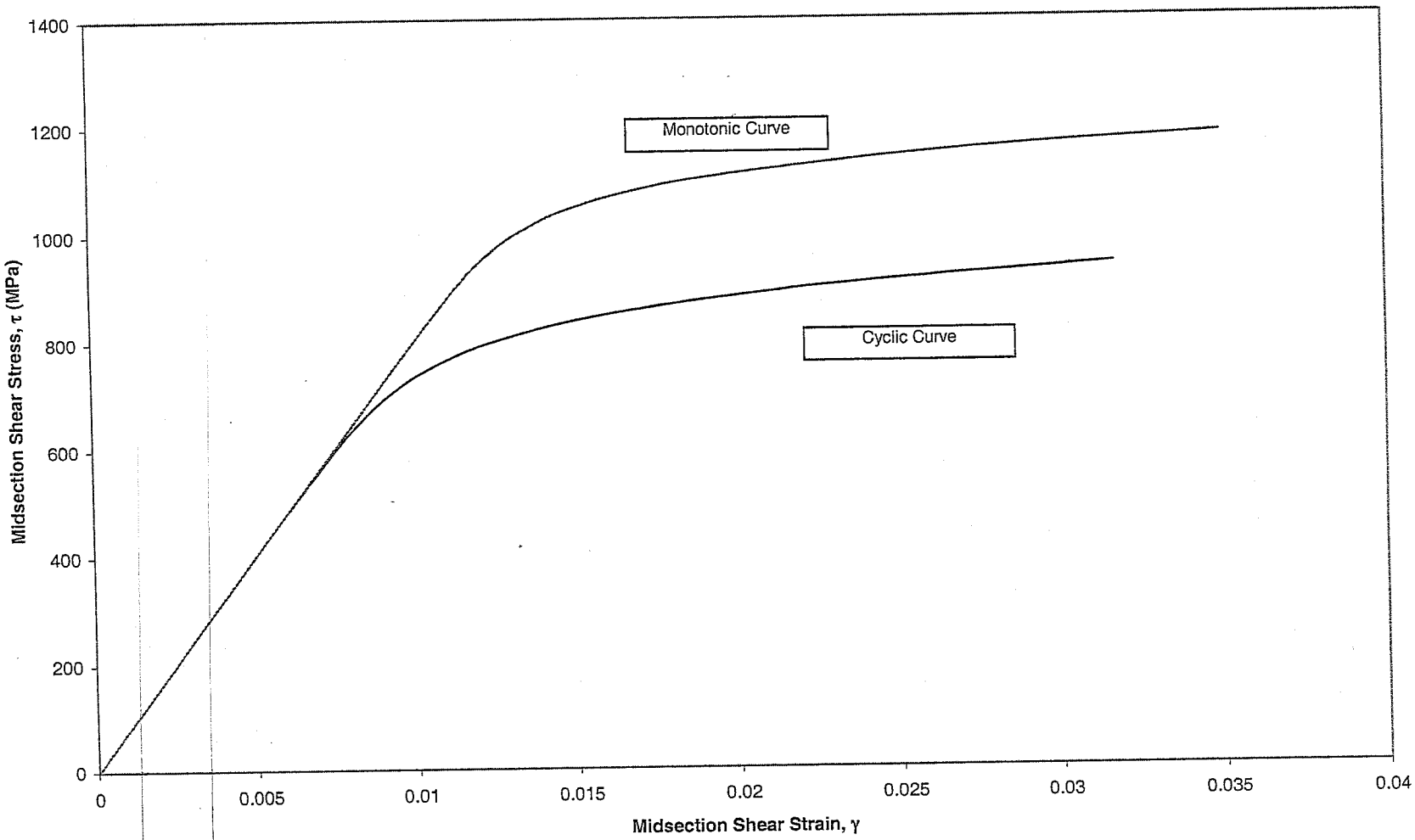

Figure 7: Composite plot of cyclic and monotonic shear stress-strain curves

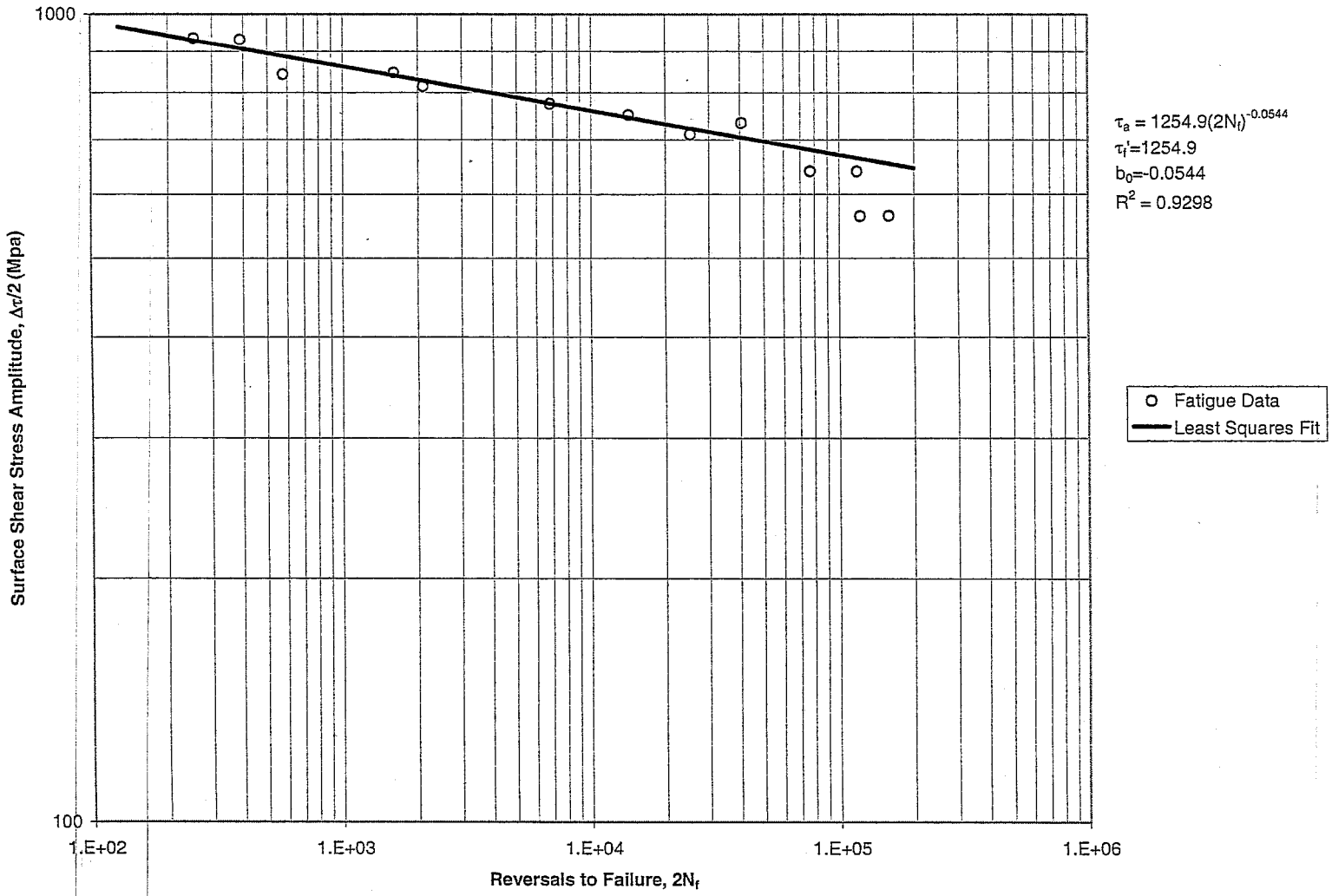

Figure 8: Shear stress amplitude versus reversals to failure

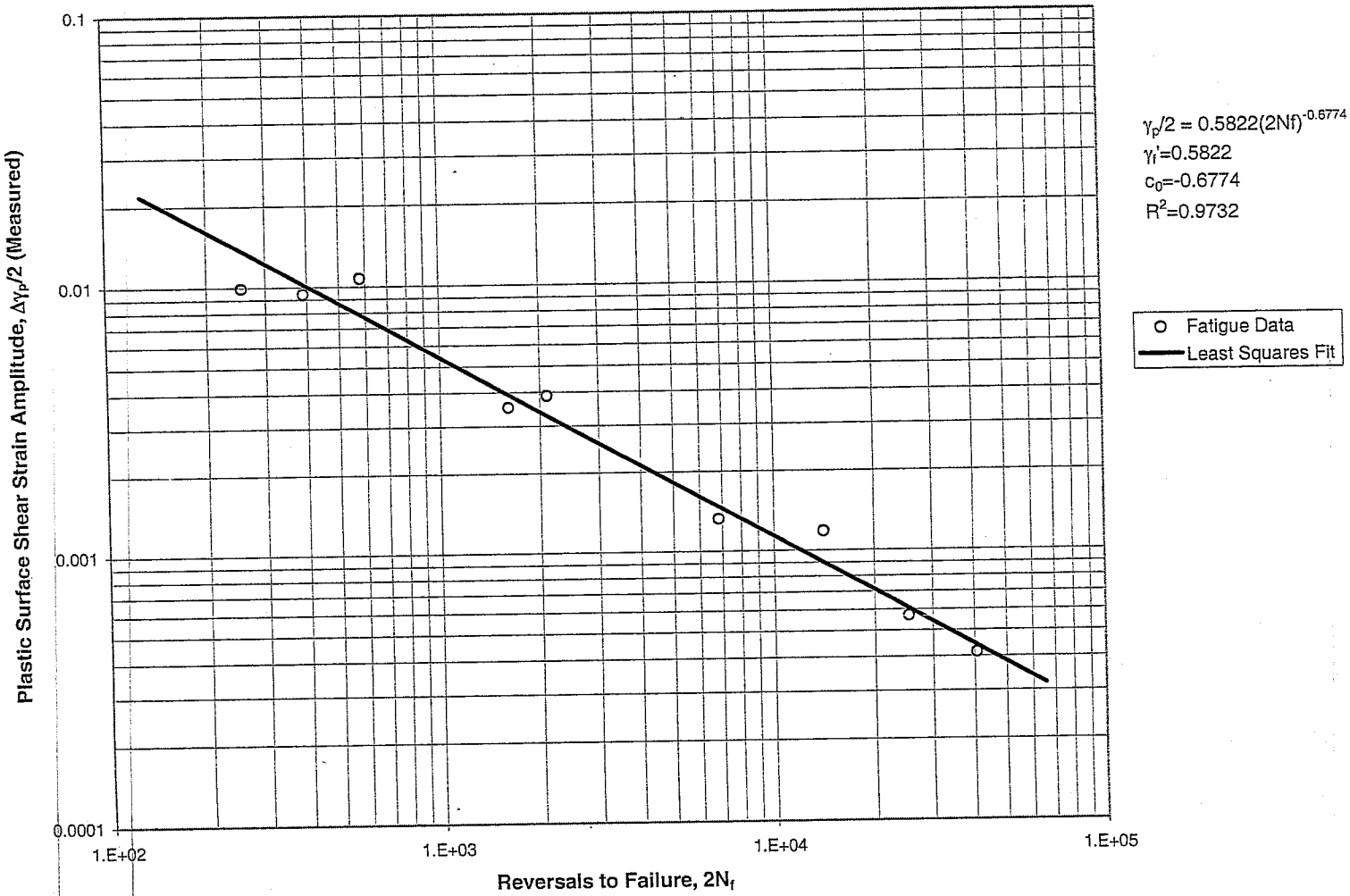

Figure 10: Measured plastic shear strain amplitude versus reversals to failure

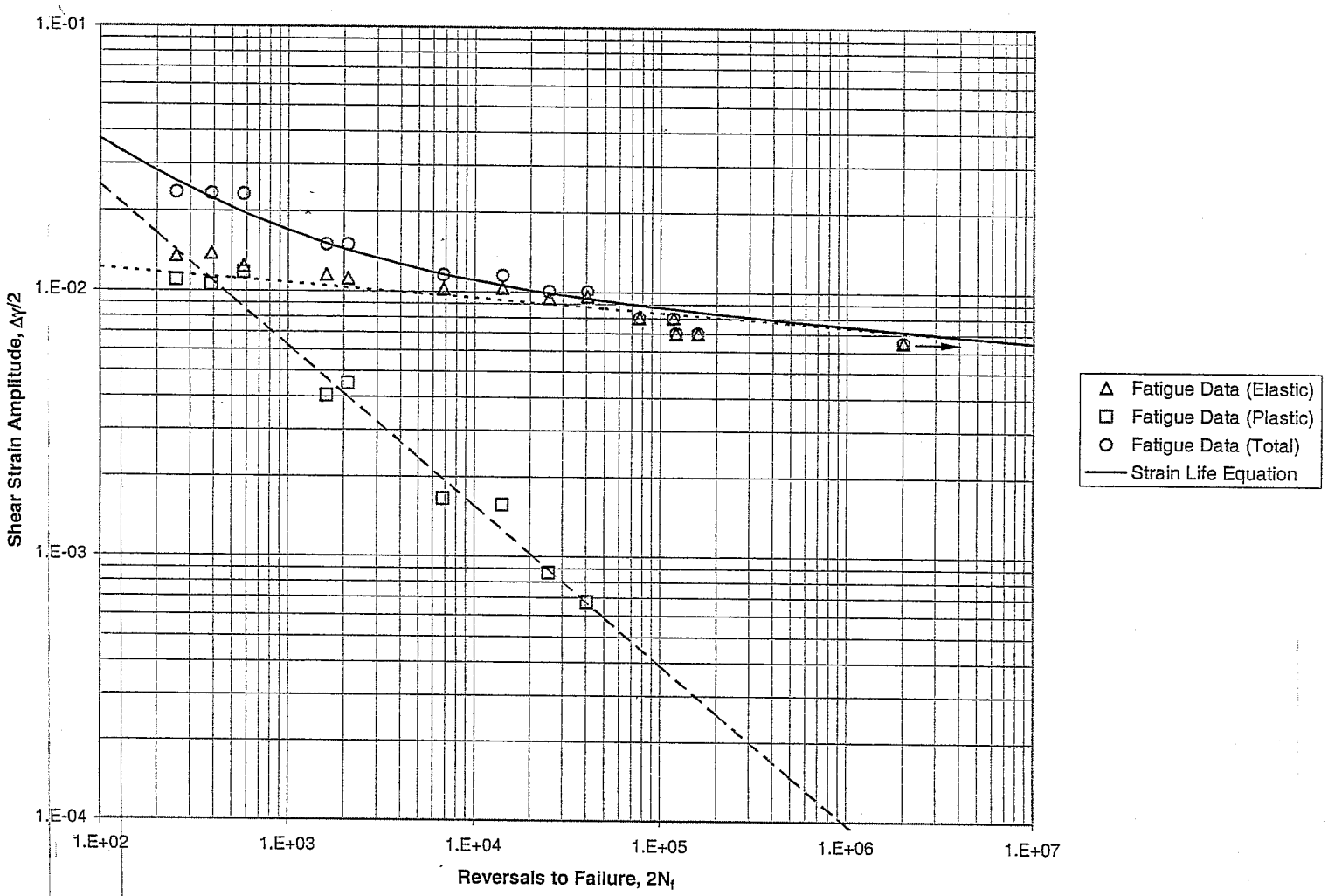

Figure 11: Shear strain amplitude versus reversals to failure

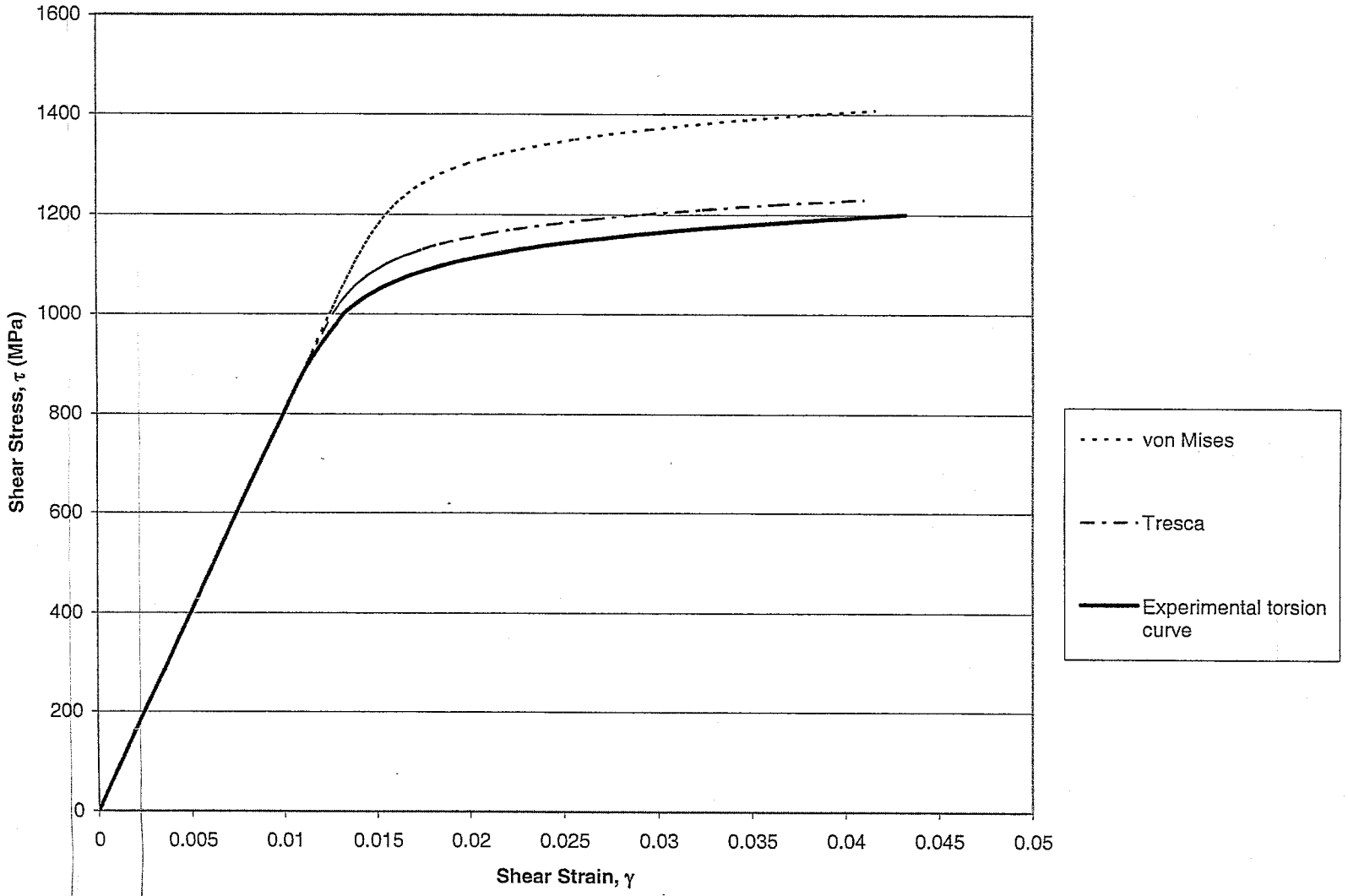

Figure 12: Comparison of monotonic torsion deformation curve with predictions based on von Mises and Tresca criteria.

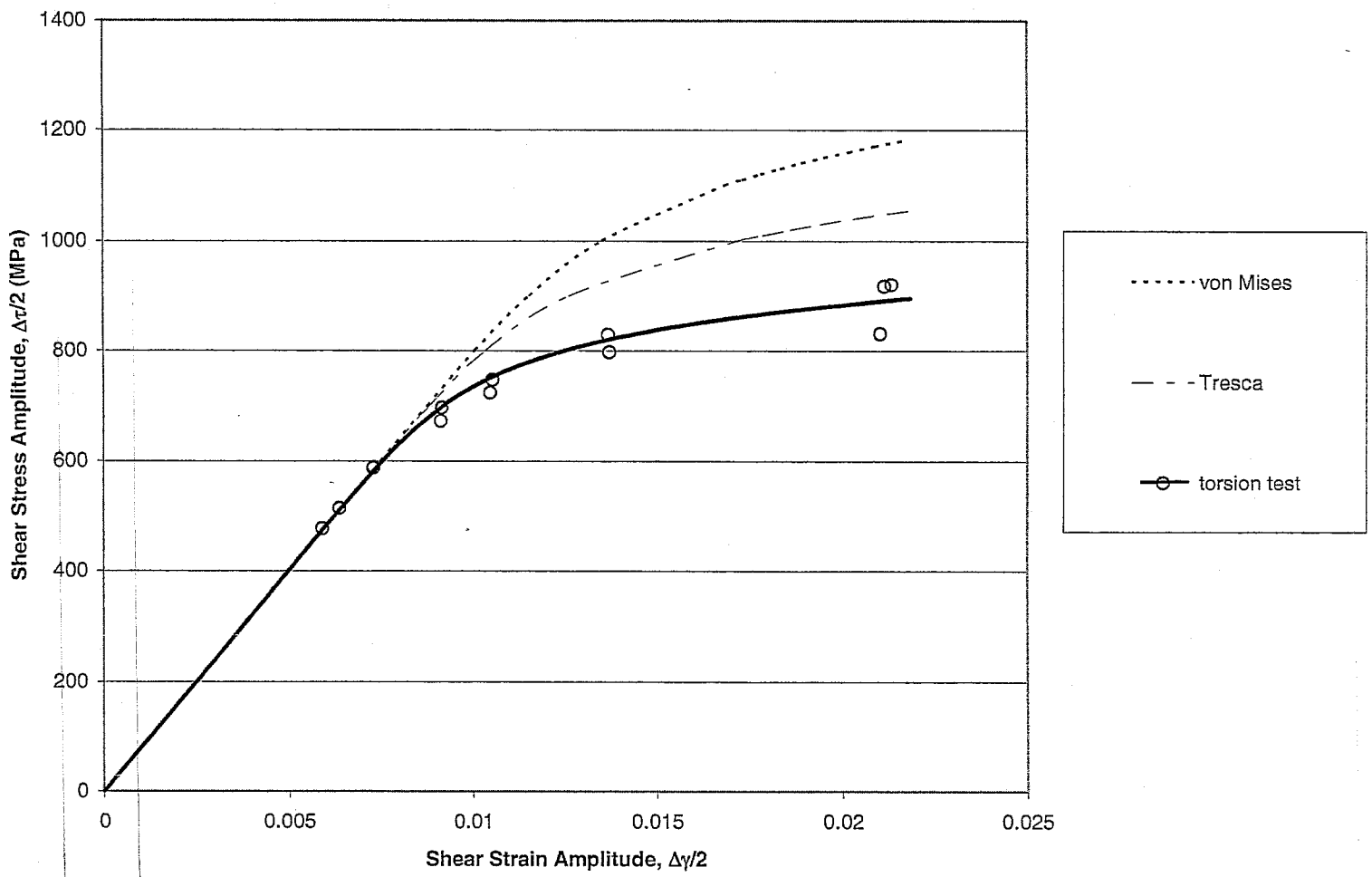

Figure 13: Torsional cyclic deformation curves based on test data and predictions

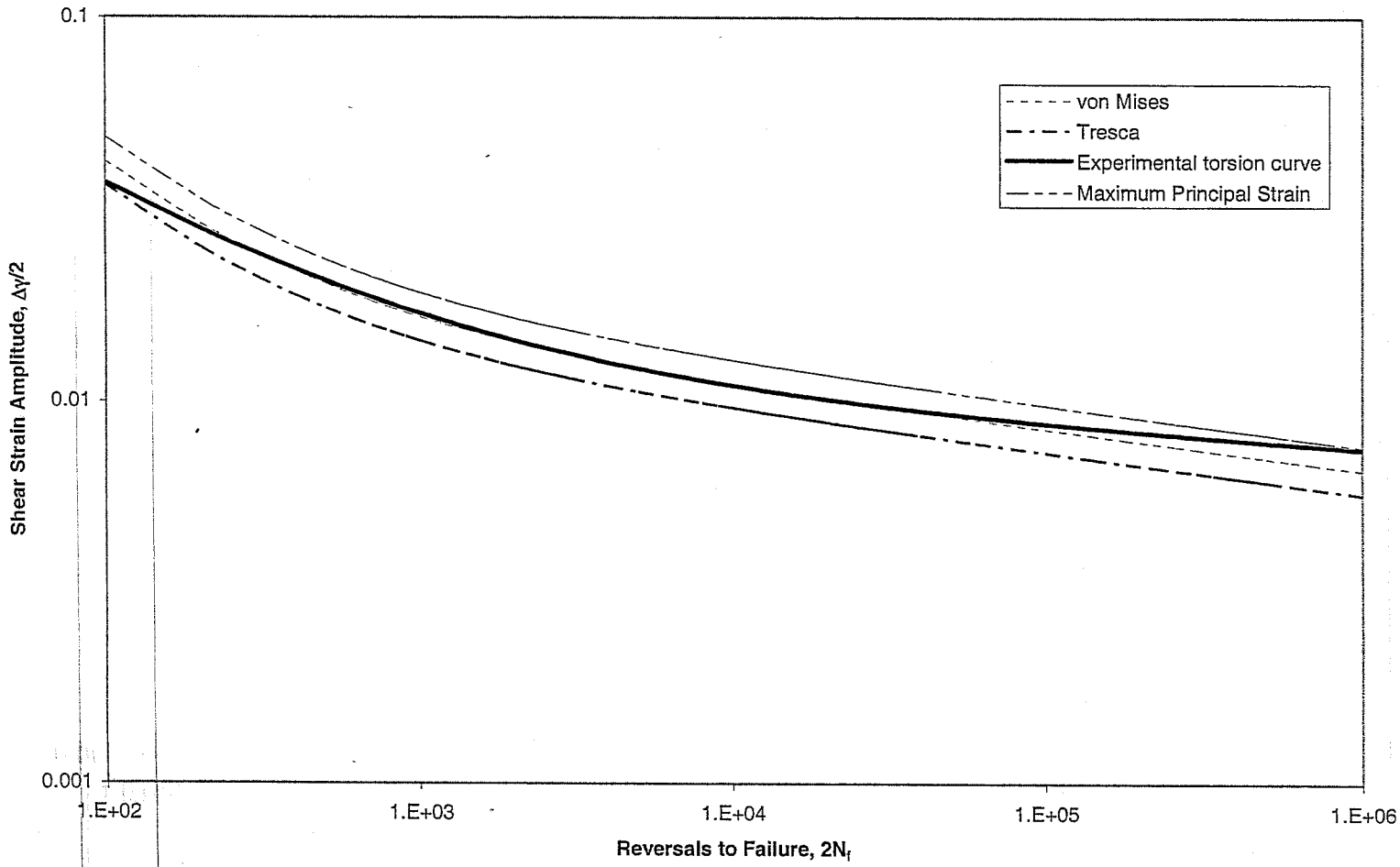

Figure 14: The total shear strain amplitude versus fatigue life from experiments and predictions

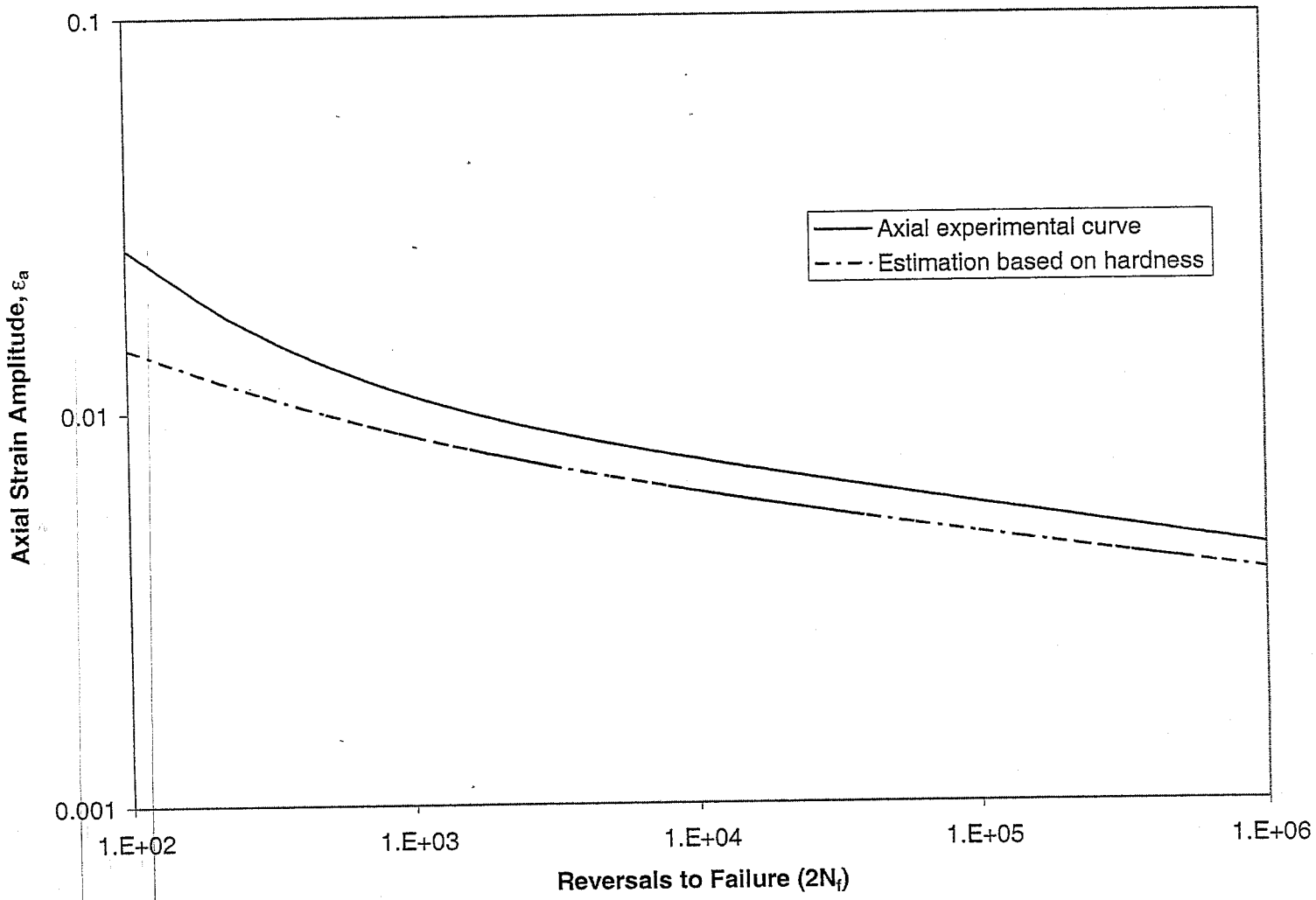

Figure 15: Comparison of experimental axial curve to axial strain-life prediction based on hardness

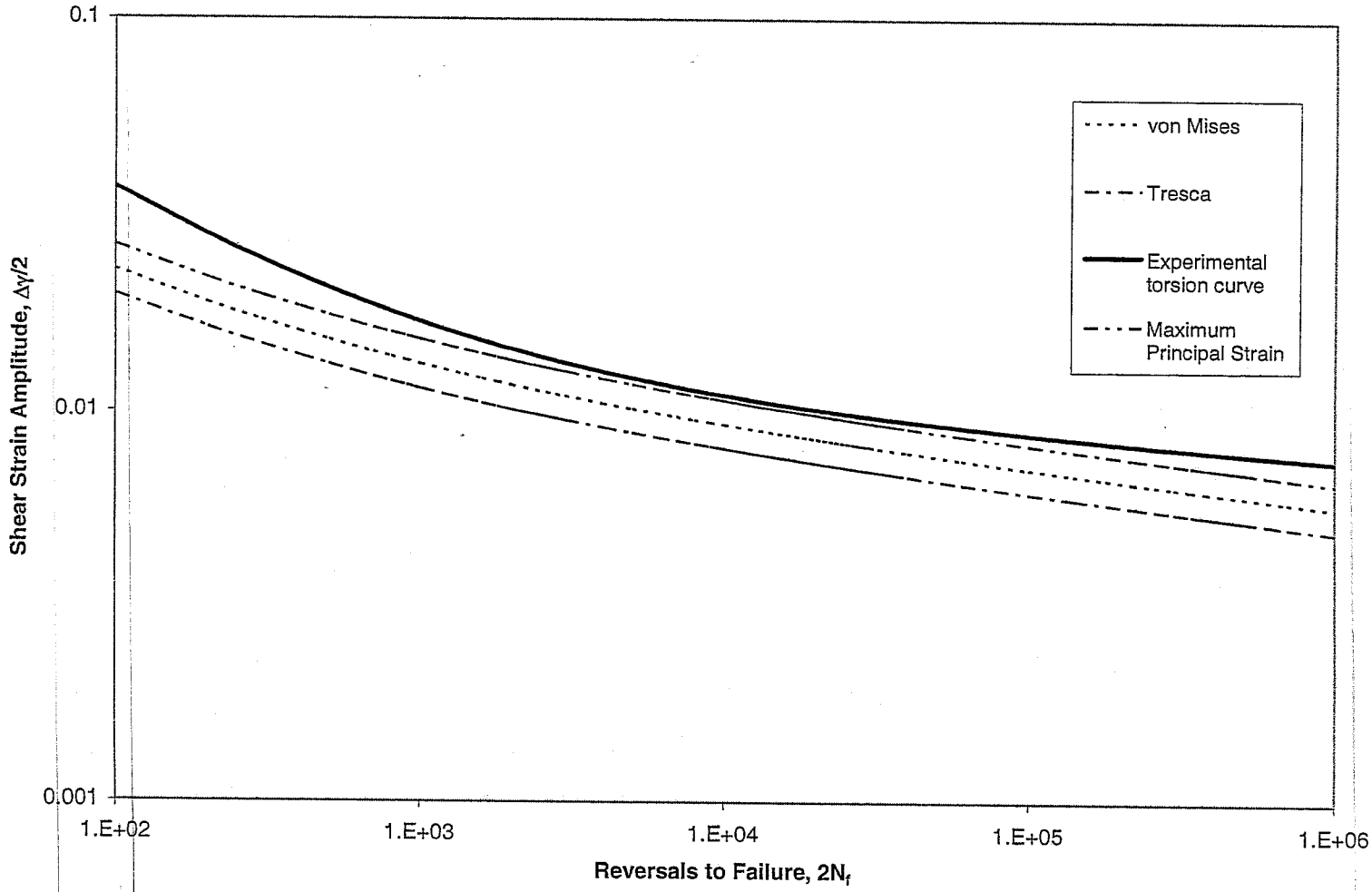

Figure 16: The total shear strain amplitude versus fatigue life from experiments and predictions using hardness

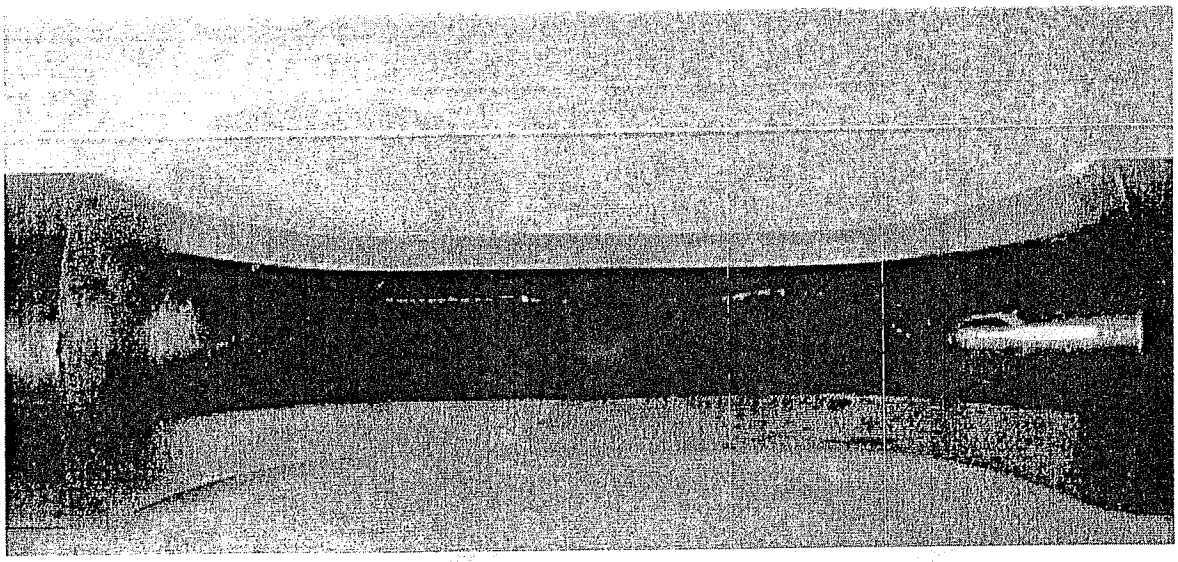

Figure 17: Unbroken specimen with longitudinal crack (specimen T 14, N_f = 3,418)

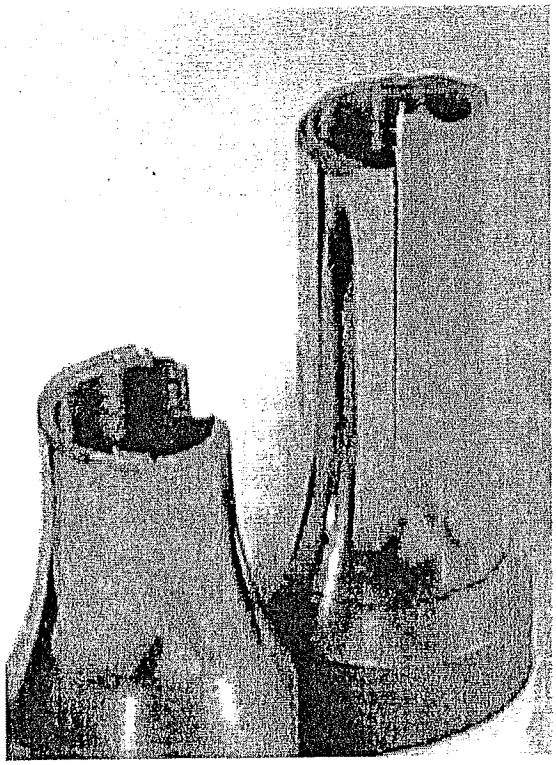

Figure 18: Fractured specimen with longitudinal crack (specimen T 7, N_f = 1,051)

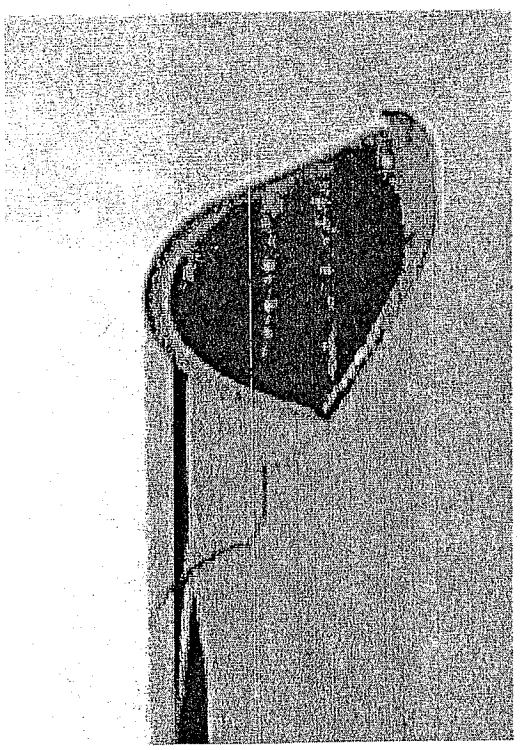

Figure 19: Fractured specimen with longitudinal crack (specimen T 11, N_f = 38,503)

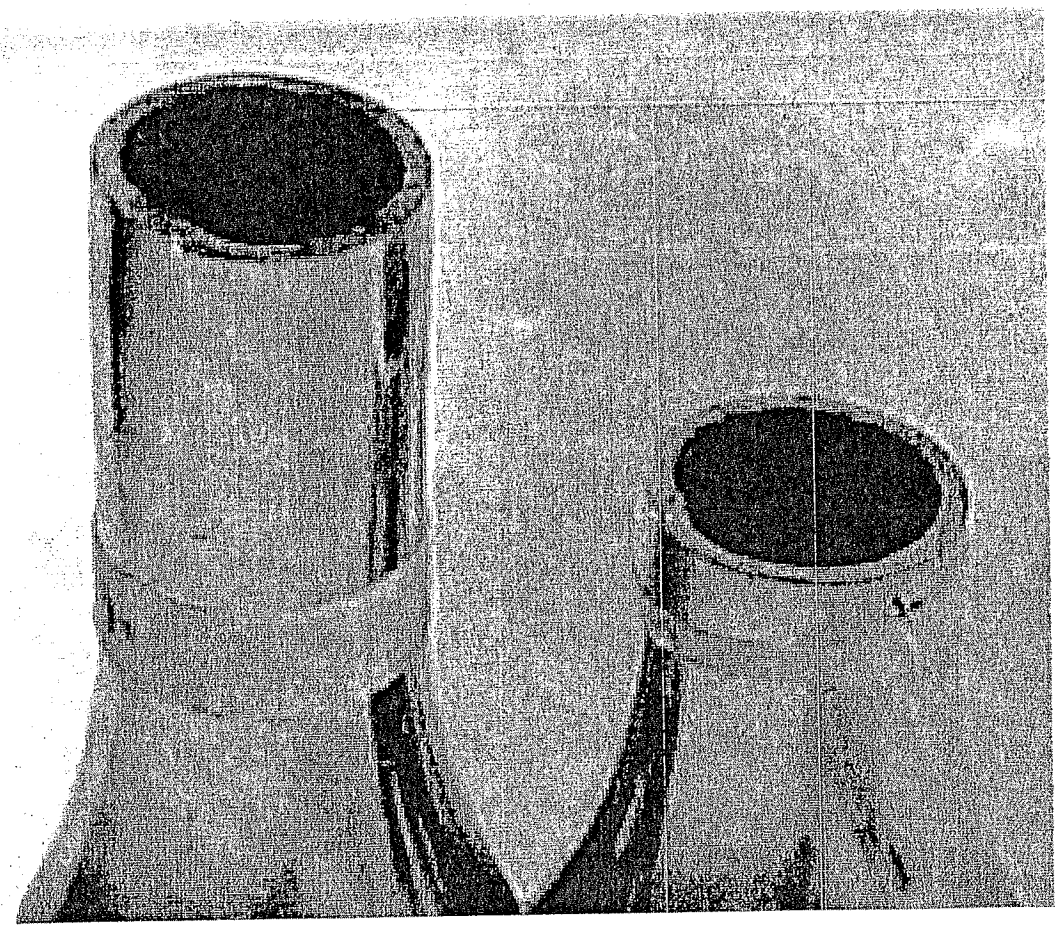

Figure 20: Fractured specimen with circumferential crack (specimen T 3, N_f = 7,088)

APPENDIX

Table A.1: Summary of Monotonic Properties for SAE 9254 AL FG Quenched and Tempered Steel

Specimen	OD, mm (in.)	ID, mm (in.)	G, GPa (ksi)	τ_y (0.2% offset), MPa (ksi)	τ_u, MPa (ksi)	K_0, MPa (ksi)	n_0	τ_f, MPa (ksi)	γ_f
T 6	15.32 (0.6031)	12.61 (0.4965)	82.6 (11985.1)	1062.6 (154.1)	1242.4 (180.2)	1459.3 (211.6)	0.0517	828.5 (120.2)	N/A
T 2	15.39 (0.6061)	12.61 (0.4966)	77.9 (11300.3)	1044.8 (151.5)	1207.1 (175.1)	1415.7 (205.3)	0.0496	1192.6 (173.0)	N/A
Average			80.3 (11642.7)	1053.7 (152.8)	1224.8 (177.6)	1437.5 (208.5)	0.0507	1010.6 (146.6)	N/A

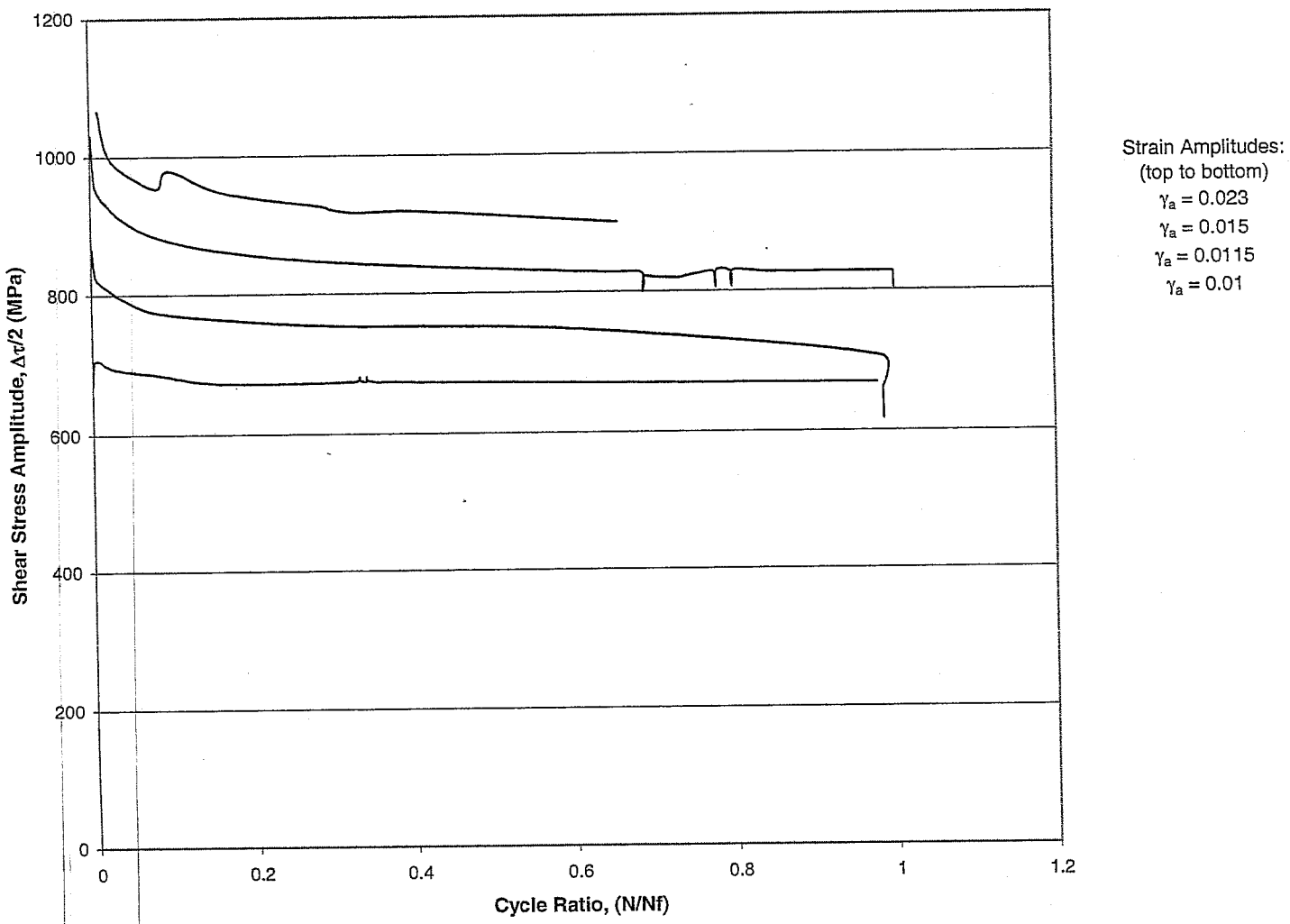

Figure A.1: Shear stress amplitude versus normalized number of cycles

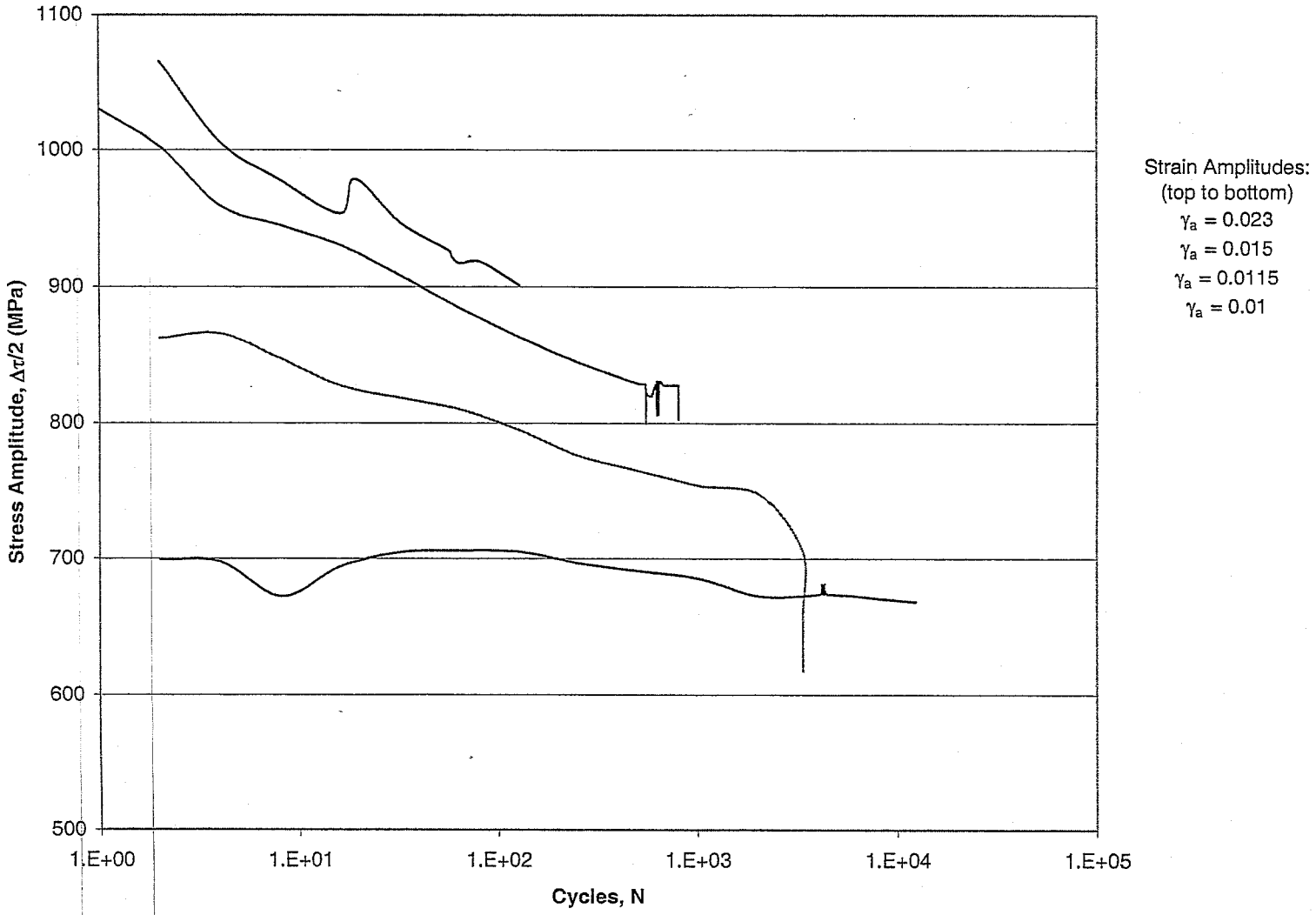

Figure A.2: Shear stress amplitude versus number of cycles

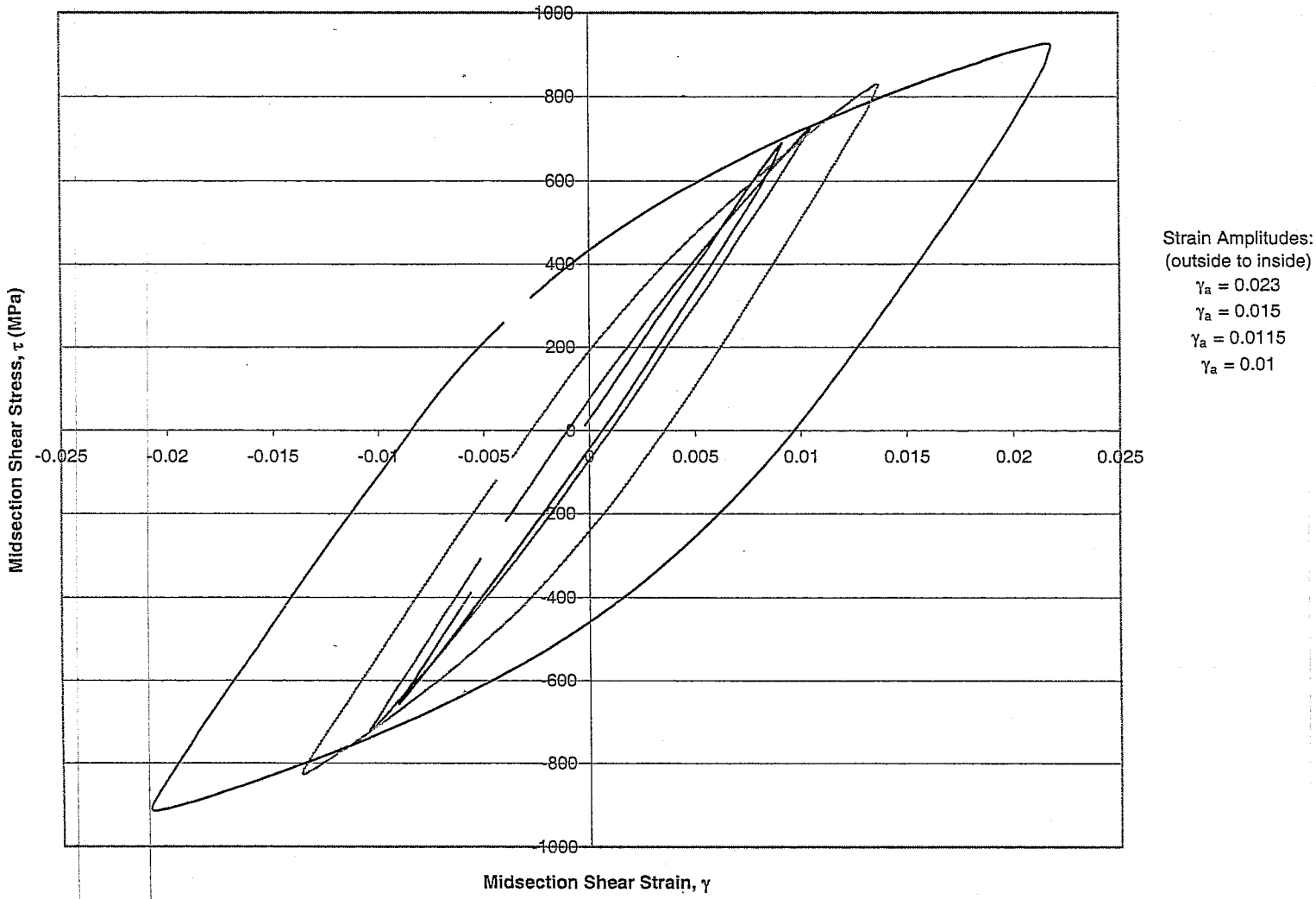

Figure A.3: Composite plot of midlife hysteresis loops